HHS Public Access

Author manuscript

Biol Psychiatry. Author manuscript; available in PMC 2022 December 01.

Published in final edited form as:

Biol Psychiatry. 2021 December 01; 90(11): 766–780. doi:10.1016/j.biopsych.2021.07.014.

Sex Differences in the Role of Cornichon Homolog-3 on Spatial Memory and Synaptic Plasticity

Hannah E. Frye[1,2,3], **Yukitoshi Izumi**[4,5,6], **Alexis N. Harris**[7], **Sidney B. Williams**[1,2], **Christopher R. Trousdale**[1,2], **Min-Yu Sun**[4], **Andrew D. Sauerbeck**[8], **Terrance T. Kummer**[8], **Steven Mennerick**[4,5,6], **Charles F. Zorumski**[4,5,6], **Elliot C. Nelson**[4], **Joseph D. Dougherty**[4,7], **Jose A. Morón**[1,2,4,5,*]

[1]Department of Anesthesiology, Washington University School of Medicine, St. Louis, MO, USA

[2]Pain Center, Washington University School of Medicine, St. Louis, MO, USA

[3]Program in Neuroscience, Washington University in St. Louis, St. Louis, MO, USA

[4]Department of Psychiatry, Washington University School of Medicine, St. Louis, MO, USA

[5]Department of Neuroscience, Washington University School of Medicine, St. Louis, MO, USA

[6]Taylor Family Institute for Innovative Psychiatric Research, Washington University School of Medicine. St. Louis, MO, USA

[7]Department of Genetics, Washington University School of Medicine, St. Louis, MO, USA

[8]Department of Neurology, Washington University School of Medicine, St. Louis, MO, USA

Abstract

Background—Cornichon homolog-3 (CNIH3) is an AMPA receptor (AMPAR) auxiliary protein prominently expressed in the dorsal hippocampus (dHPC), a region that plays a critical role in spatial memory and synaptic plasticity. However, effects of CNIH3 on AMPAR-dependent synaptic function and behavior have not been investigated.

Methods—We assessed a gain-of-function model of *Cnih3* overexpression in the dHPC and generated and characterized a line of *Cnih3*$^{-/-}$ C57BL/6 mice. We assessed spatial memory through behavioral assays, protein levels of AMPAR subunits and synaptic proteins by immunoblotting, and long-term potentiation (LTP) in electrophysiological recordings. We also utilized a super-resolution imaging workflow, SEQUIN, for analysis of nanoscale synaptic connectivity in dHPC.

[*]**Corresponding author:** Dr. Jose A. Morón, jmoron-concepcion@wustl.edu), Phone: (314) 362-0078, Mailing Address: 660 S. Euclid Avenue, Campus Box 8054, St. Louis, MO 63110.

DISCLOSURES

C.F.Z. serves on the Scientific Advisory Board and owns stock in Sage Therapeutics. Other authors report no biomedical financial interests or potential conflicts of interest.

Results—Overexpression of *Cnih3* in dHPC improved short-term spatial memory in female mice, but not in male mice. *Cnih3*$^{-/-}$ female mice exhibited weakened short-term spatial memory, reduced dHPC synapse density, enhanced expression of calcium-impermeable AMPAR (GluA2-containing) subunits in synaptosomes, and attenuated LTP maintenance compared to *Cnih3*$^{+/+}$ controls; *Cnih3*$^{-/-}$ males were unaffected. Further investigation revealed that deficiencies in spatial memory and changes in AMPAR composition and synaptic plasticity were most pronounced during the metestrus phase of the estrous cycle in female *Cnih3*$^{-/-}$ mice.

Conclusion—This study identified a novel effect of sex and estrous on CNIH3's role in spatial memory and synaptic plasticity. Manipulation of CNIH3 unmasked sexually dimorphic effects on spatial memory, synaptic function, AMPAR composition, and hippocampal plasticity. These findings reinforce the importance of considering sex as a biological variable in studies of memory and hippocampal synaptic function.

Keywords

sex differences; memory; AMPA receptors; hippocampus; synaptic plasticity; super-resolution microscopy

INTRODUCTION

The glutamatergic AMPA receptor (AMPAR) is widely expressed in the central nervous system and is an essential component of the mechanisms underlying synaptic plasticity and memory (1). AMPARs are highly regulated by auxiliary proteins which regulate trafficking, subunit composition, glutamate sensitivity, and membrane stabilization (1–4). Cornichon homolog-3 (CNIH3) is one such AMPAR auxiliary protein in the brain (5–9), however, little is known about how it impacts mammalian behavior.

The CNIH proteins CNIH2 and CNIH3 serve as AMPAR chaperones to the synaptic membrane and as auxiliary proteins which enhance AMPAR activity (5 – 18). However, as CNIH2 is expressed at a higher level in the brain than CNIH3 (5, 19), most studies have either investigated CNIH2 alone or the cumulative effects of both CNIH2/3; significantly less is known about CNIH3-specific effects. In addition, prior studies of CNIH2/3 function were not designed to detect potential effects of sex, an important limitation given previously identified sex differences in glutamatergic signaling (20) and the imperative of considering sex as a biological variable (SABV) in biomedical research (21).

In addition to CNIH2/3, additional AMPAR auxiliary proteins such as transmembrane AMPAR regulatory proteins (TARPs) (3, 4, 6, 22), CKAMPs (23), and GSG1L (24, 25) are important components of AMPAR machinery in the brain. These AMPAR auxiliary subunits contribute to a wide range of behaviors and psychiatric disorders (2, 3, 26, 27), such as motor activity and epilepsy (28), pain sensitization (29), memory (30), drug-associated behavior (31 – 33), social behaviors (34), and stress (35). Despite the established links between AMPAR auxiliary proteins and behavior, only a small number of studies have explored the role of CNIH proteins on mammalian behavior. Variations in *CNIH* gene expression have been associated with elevated schizophrenia risk (36) and intellectual disability (37). Interestingly, *CNIH3*, but not *CNIH2*, was linked with reduced

risk for opioid use disorder (38). However, no studies have addressed how CNIH3 may contribute to these disorders. As we have previously reported on the role of AMPARs and the dorsal hippocampus (dHPC) on learning and memory in mice (32, 39–43), we hypothesized that CNIH3 plays a key role in spatial memory, synaptic connectivity, and synaptic plasticity. Across modalities ranging from biochemical, physiological, structural, and behavioral studies, our results uncovered marked effects of both sex and estrous cycling on CNIH3-dependent spatial memory, synaptic connectivity, AMPAR subunit composition, and plasticity in the dHPC.

MATERIALS AND METHODS

Animals

Procedures were approved by the Institutional Animal Care and Use Committee at Washington University in St. Louis. Adult (8 – 16 weeks) male and female C57BL/6 wild-type (WT, *Cnih3*$^{+/+}$), *Cnih3*$^{tm1a(KOMP)Wtsi}$, and *Cnih3* knockout (KO, *Cnih3*$^{-/-}$) mice were kept in climate-controlled facilities with a 12-hour light/dark cycle and *ad libitum* access to food and water.

β-galactosidase staining

To visualize the anatomical expression of the *Cnih3*$^{tm1a(KOMP)Wtsi}$ gene in the brain, we stained the brains of homozygous mutant mice for the *lacZ* cassette contained within the *Cnih3*$^{tm1a(KOMP)wtsi}$ gene using a β-galactosidase staining assay as previously described (44, 45). A detailed staining protocol is provided in the Supplemental Materials.

Viral intracranial injection surgeries for Cnih3 overexpression

Surgeries for intracranial viral injection of AAV5-CAMKII-myc-CNIH3-t2a-GFP and AAV5-CAMKII-eYFP viruses in the dHPC are described in the Supplemental Materials.

Real-time quantitative PCR (RT-qPCR)

RT-qPCR protocols are included in the Supplemental Materials.

Barnes maze spatial memory task

To assess changes in spatial learning and memory, we performed a Barnes maze spatial learning task as previously described (42). A detailed description of this protocol is provided in the Supplemental Materials. Following habituation and training (Days 0 – 4) on a Barnes maze circular platform surrounded by distinct visual cues, on Days 5 and 12, a 90 s probe trial was conducted. The latency to the first target hole entry (primary latency), number of errors made prior to target hole entry (primary errors), and the path efficiency (distance traveled to target / shortest possible distance) were recorded. The estrous cycle was monitored daily in female animals during testing (Figure S1).

Western blotting

Dorsal and ventral hippocampi were collected and whole-cell homogenate and synaptosomal fractions were obtained and processed as previously described (32, 46, 47). A detailed western blot protocol is included in the Supplemental Materials.

Synapse quantification with SEQUIN multiscale imaging

A detailed description and validation of SEQUIN (Synaptic Evaluation and QUantification by Imaging of Nanostructure) can be found in the technique's original manuscripts by Sauerbeck et al., 2020 (48) and Reitz et al., 2021 (49); and in the Supplemental Materials and Figure S9. The SEQUIN code (Matlab, Mathworks) is available here: GitHub https://github.com/KummerLab/SEQUIN (48, 49).

Field excitatory postsynaptic potentials (fEPSPs) and long-term potentiation (LTP)

Female *Cnih3*$^{+/+}$ and *Cnih3*$^{-/-}$ mice aged 6-8 weeks were monitored daily for estrous cycling, and mice in the metestrus stage were selected for Schaffer Collateral (SC) LTP experiments (50). A detailed protocol for these experiments is provided in the Supplemental Materials.

Statistics and analysis

Results are presented as the mean ± SEM. Datasets were analyzed using GraphPad Prism 9 software. Normal datasets (determined by the Shapiro-Wilk test) were analyzed by unpaired two-tailed *t* tests (two groups) or one-way ANOVA (≥ three groups) followed by *post-hoc* Sidak's multiple comparisons test. Non-normal datasets were analyzed by a two-tailed Mann-Whitney U test (two groups) or by a Kruskal-Wallis test (≥ three groups) followed by *post-hoc* Dunn's multiple comparisons test. Datasets comparing two factors were compared using a two-way ANOVA followed by *post-hoc* Sidak's multiple comparisons test. Outliers were determined within each dataset using a Grubbs' Outlier test and are specified for each experiment in Table S1. Statistical significance is represented as ns $p > 0.05$, * $p < 0.05$, ** $p < 0.01$, *** $p < 0.001$, and **** $p < 0.0001$. Datasets were considered statistically significant with $p < 0.05$.

EXPERIMENTAL RESULTS

LacZ-tagged Cnih3 prominently expressed in the hippocampus

To identify anatomical expression of *Cnih3* in the brain, we used a β-galactosidase staining assay to visualize the *lacZ* cassette contained within the *Cnih3*$^{tm1a(KOMP)wtsi}$ gene of *Cnih3*$^{tm1a(KOMP)Wtsi}$ mice (51) (Figure 1A). No *lacZ* staining was observed in WT *lacZ*- brains (Figure 1B). In *lacZ*+ brains, *LacZ* reporter expression was strongest in the prefrontal cortex (PFC), hypothalamus, cortical regions, amygdala, and hippocampus (Figures 1C – E, males and females) (19). Within the hippocampus, *LacZ* reporter expression was especially pronounced within the Dentate Gyrus (DG) and CA1 (Figure 1F). These results concurred with previous studies which also reported prominent expression of *Cnih3* expression in the hippocampus (5, 14, 19).

Validation of a new Cnih3 viral overexpression construct

To investigate the effect of localized *Cnih3* overexpression, we generated an AAV5-CAMKII-myc-CNIH3-t2a-GFP virus to overexpress *Cnih3.* The dHPC of mice injected with the *Cnih3* overexpression virus (Figure 2A) expressed ~500X more *Cnih3* mRNA than YFP-injected controls (Figure 2B). We observed a small decrease in *Cnih2* expression in the dHPC of *Cnih3* overexpressing animals compared to YFP-injected controls (Figure 2B, no differences between male and female samples). To verify the location of viral expression and monitor viral spread, brain slices were stained for the myc-tag adjacent to CNIH3 in the AAV5-CAMKII-myc-CNIH3-GFP construct (Figure 2C).

Spatial memory is improved in female mice overexpressing Cnih3 in the dHPC

To assess whether hippocampal CNIH3 can modulate spatial memory, an AMPAR-mediated process (52–56), we induced viral overexpression of *Cnih3* in the dHPC of male and female mice and tested animals in a Barnes maze spatial memory task (Figure 2D – E, Figure S2).

During the short-term probe trial, performance in the Barnes maze task was strongly affected by both animal sex and virus expressed. Female mice overexpressing *Cnih3* in the dHPC committed fewer primary errors, had a shorter latency to reach the target, and took more direct routes to the target compared to YFP-expressing females (Figure 2F – H). We did not observe any differences between YFP-expressing males and *Cnih3* overexpressing males nor between male and female YFP controls (Figure 2F – H). During the long-term probe trial, performance in the Barnes maze was not affected by sex nor virus expressed (Figure 2I – K). No differences in memory were observed due to estrous cycling in females (Figure S3).

These experiments demonstrated that targeted overexpression of *Cnih3* in the dHPC improved short-term spatial memory in the Barnes maze task only in female mice.

Generation and validation of a Cnih3 knockout (KO) mouse line

To further explore the role of CNIH3 in spatial memory and underlying memory mechanisms, we sought to generate a functional *Cnih3* KO mouse line. *Cnih3*$^{tm1a(KOMP)wtsi}$ mice, obtained from the Knockout Mouse Project (51), contained a polyadenylation (pA) site following exon 3 in *Cnih3* to attenuate transcription (Figure 3A). However, *Cnih3*$^{tm1a(KOMP)wtsi}$ HET and HOM animals only expressed a 60% reduction in exon 4 of *Cnih3* (Figure 3B). We observed no change in *Cnih2* expression across genotypes.

To create full *Cnih3* KO animals, we conducted additional breeding of *Cnih3*$^{tm1a(KOMP)wtsi}$ to excise exon 4 (Figure 3C), resulting in a frameshift mutation across exons 5 and 6 and a truncation of CNIH3 translation. *Cnih3*$^{-/-}$ mice presented a total elimination of *Cnih3* exon 4 (Figure 3D, no differences between male and female samples). *Cnih2* expression remained unchanged in *Cnih3*$^{+/-}$ and *Cnih3*$^{-/-}$ mice.

Spatial memory is impaired in Cnih3$^{-/-}$ female mice

To determine if CNIH3 is necessary for spatial memory in female mice, we tested *Cnih3*$^{+/+}$, *Cnih3*$^{+/-}$, and *Cnih3*$^{-/-}$ mice in the Barnes maze spatial memory task (Figure 4A, Figure S4). During the short-term probe trial (Figures 4B – D), performance in the Barnes

maze was strongly affected by the interaction of sex and genotype. *Cnih3*$^{-/-}$ female mice committed more primary errors, had a higher primary latency to reach the target, and displayed decreased path efficiency to the target compared to *Cnih3*$^{+/+}$ females (Figure 4B–D). No differences in spatial memory were observed between males of any genotype nor between male and female *Cnih3*$^{+/+}$ animals. In the long-term probe on day 12 of the Barnes maze task, no differences in Barnes maze performance were observed across groups (Figures 4E – G).

These experiments demonstrated that *Cnih3* KO attenuated short-term spatial memory in in female, but not male, animals, an intriguing counterpoint to the enhanced short-term memory in *Cnih3* overexpressing females (Figure 2).

Spatial memory impairment in female Cnih3$^{-/-}$ mice occurs primarily during the metestrus stage of the estrous cycle

Given the reported interactions between estrous cycling and hippocampal AMPAR activity (57, 58), we assessed whether the estrous cycle influenced short-term spatial memory in naturally cycling *Cnih3*$^{-/-}$ female mice (Figure S1). We observed pronounced effects of both genotype and estrous cycle stage on spatial memory in the Barnes maze (Figures 4H – J, see also Figure S5). Spatial memory attenuation was strongest in *Cnih3*$^{-/-}$ female animals during the metestrus stage of the estrous cycle. No differences were observed across estrous cycle stages in *Cnih3*$^{+/+}$ nor *Cnih3*$^{+/-}$ female animals (Figure 4H – J), with no memory differences during the long-term probe in any genotype (Figure S6).

Gene expression of Cnih3 and related genes are unaffected by estrous cycle stage

Next, we investigated whether natural estrous cycling affects gene expression of *Cnih3* and associated genes in the dHPC. There were no changes due to sex or estrous cycle in *Cnih3, Cnih2, Gria1*, or *Gria2* expression, but there was increased expression of *Dlg4* in females overall (Figure S7). *Dlg4* encodes for the post-synaptic structural scaffolding protein PSD-95, which is critical for anchoring receptors (including AMPARs) and ion channels at the synapse (60).

Synaptic connectivity is disrupted in Cnih3$^{-/-}$ female animals

Changes in synaptic structural proteins can indicate altered synaptic structural dynamics that underlie memory formation in the dHPC (61–64). Therefore, one possible explanation for the impaired memory formation in the dHPC is a reduction in memory storing synapses in *Cnih3*$^{-/-}$ females. Thus, we examined expression levels of the postsynaptic marker PSD-95 and the presynaptic marker synapsin-1 in dHPC homogenate samples obtained from *Cnih3*$^{+/+}$ and *Cnih3*$^{-/-}$ mice (Figure 5A).

PSD-95 expression in the dHPC as measured by western blot did not differ between *Cnih3*$^{+/+}$ and *Cnih3*$^{-/-}$ male or female mice nor between estrous cycle stages (Figure 5B). We also observed no differences due to sex or estrous cycle stage on PSD-95 expression in synaptosomal fractions from the dHPC and from the vHPC (Figure S8). However, we observed reduced synapsin-1 expression in the dHPC only in *Cnih3*$^{-/-}$ female mice, particularly during metestrus (Figure 5C). In addition, we observed a similar decrease of

synapsin-1 in the vHPC of female *Cnih3*$^{-/-}$ mice during the metestrus stage, a region which also mediates learning and memory (Figure S9). While we previously observed an overall increase in the expression of the PSD-95 encoding gene *Dlg4* in the dHPC of female WT mice compared to males (Figure S7), our data indicate no changes in basal PSD-95 protein levels in the dHPC due to sex (Figure 5B).

These alterations in structural synaptic proteins in female *Cnih3*$^{-/-}$ mice suggested there may be a disruption in synapses in the dHPC. We investigated synaptic connectivity in the CA1 region of the dHPC utilizing a newly developed super-resolution protocol for the quantification of synaptic loci: SEQUIN (48). Slices from *Cnih3*$^{+/+}$ and *Cnih3*$^{-/-}$ male and female mice were stained for synapsin and PSD-95, followed by super-resolution imaging with Airyscan detection (Figure 5D – E and S10) to detect pre-to-postsynaptic nearest-neighbor (NN) synaptic pairs. The frequency distribution of NN pairs revealed a sharp early peak (<400 μm), representing synaptic loci, in addition to a broader random pairing peak at higher separation distances (Figure 5F). Random NN pairs were removed as described (Supplemental Materials & Figure S10) to quantify paired puncta associated with synaptic loci (Figure 5G).

Upon closer inspection of the NN paired frequency distributions, we observed increased NN separation of pre-to-postsynaptic pairs in female *Cnih3*$^{-/-}$ samples (Figure 5F – H). No difference in separation distance was observed between male *Cnih3*$^{+/+}$ and *Cnih3*$^{-/-}$ samples, but the NN separation was decreased in *Cnih3*$^{+/+}$ females compared to *Cnih3*$^{+/+}$ males, suggesting that CNIH3 in females may interact with synaptic mechanisms to tighten pre- to postsynaptic connectivity.

Due to the limited resolution of western blotting for precise quantification of protein expression, we also utilized SEQUIN imaging to assess the density of structural synaptic proteins in the CA1 of the dHPC. Female *Cnih3*$^{-/-}$ mice displayed a lower density of both PSD-95 and synapsin puncta compared to female controls in the dorsal CA1 (Figure 5I – J). No differences were observed between male and female *Cnih3*$^{+/+}$ samples for PSD-95, but female *Cnih3*$^{+/+}$ mice displayed increased synapsin density compared to male controls.

To assess whether CNIH3 and animal sex modulate overall synaptic density, we quantified NN pre- and postsynaptic pairs associated with synaptic loci. Slices from *Cnih3*$^{-/-}$ females had a lower density of synaptic loci compared to *Cnih3*$^{+/+}$ females. No differences in the density of synaptic loci were observed in the dorsal CA1 of male samples, nor between male and female *Cnih3*$^{+/+}$ samples (Figure 5K). Our data also revealed stretched NN separation distances in the dorsal CA1 of *Cnih3*$^{-/-}$ females, indicating a potential shift in the localization of these proteins within the synapse or reduced connectivity between pre- and postsynaptic matrices, which could lead to defects in neurotransmission and synapse stability (65, 66).

Synaptosomal AMPAR subunit composition is altered in the dHPC of Cnih3$^{-/-}$ female mice during metestrus

Prior biochemical studies have dissected the interaction between CNIH proteins and AMPAR subunits at length, but these studies either investigated only the role of CNIH2

(5, 14), did not distinguish between CNIH2/3 (6), or did not specifically investigate the individual role of CNIH3 on AMPARs in the hippocampal region (7). None of these studies distinguished samples by sex. Therefore, we investigated whether CNIH3 affected AMPAR subunit composition in the dHPC in a sex-dependent manner.

First we assessed the role of CNIH3 on the expression of the GluA1 subunit in the dHPC at the synaptosome (Figure 6A). We did not observe any changes in male or female dHPC synaptosomal GluA1 expression or in GluA1 S845 phosphorylation, which signals for receptor insertion in the membrane (67, 68) (Figure 6B – C). However, we did observe a slight increase in GluA1 S845 phosphorylation due to estrous cycle stage independent of genotype (Figure 6C). For both GluA1 and phospho-GluA1 Ser845, we observed no differences between male and female controls.

Next we investigated the role of CNIH3 on the expression of the GluA2 subunit in the synaptosome (Figure 6D). We observed a slight increase in GluA2 expression in the dHPC of female *Cnih3*$^{-/-}$ samples which was most pronounced during metestrus (Figure 6E). We did not observe differences in synaptosomal GluA2 Y876 phosphorylation, which triggers the removal of GluA2-containing AMPARs from the synapse (69), in the dHPC of any group (Figure 6F). We did not observe any changes in AMPAR subunit composition or phosphorylation in vHPC synaptosomal fractions from female mice (Figure S11), a region which plays a key role in non-spatial learning and memory processes (70, 71). These data suggest a degree of regional specificity for CNIH3 modulation of AMPAR subunit composition within the hippocampus.

Together, these data suggest that the interaction in the dHPC between CNIH3 and AMPAR subunits may be differentially modulated by fluctuations in endogenous sex hormones. Without CNIH3 available to assist in normal AMPAR trafficking and signaling during metestrus, AMPAR composition skewed toward calcium-impermeable GluA2-containing receptors. This shift in AMPAR subunit composition may result in disrupted AMPAR-reliant processes such as synaptic plasticity, where the exchange of GluA1 and GluA2 AMPAR subunits is critical to the induction and maintenance of LTP.

LTP maintenance is disrupted in the Schaffer Collateral (SC) pathway of Cnih3$^{-/-}$ female mice

We examined the role of CNIH3 in on synaptic activity and plasticity to investigate how changes in AMPAR subunit composition, observed only in *Cnih3*$^{-/-}$ female animals during metestrus, may affect hippocampal mechanisms underlying memory. During initial experiments, we did not observe any effects of CNIH3 on miniature excitatory postsynaptic currents (mEPSCs) in slices obtained from juvenile, pre-cycling mice (P17-21) (Figure S12). This finding concurs with prior studies from Herring *et al.*, 2013, which only reported acute electrophysiological impairments in slice preparations obtained from juvenile (<P21) *Cnih2* and dual *Cnih2/3* KO mice (male and female combined) (5). However, as our behavioral and biochemical data suggest a potential interaction between CNIH3 and hormonal cycling in females on memory and AMPAR regulation, we sought to further investigate the role of CNIH3 on synaptic plasticity in the dHPC of sexually mature, naturally cycling female mice.

For the first experiment, we used a single 100 Hz x 1 s HFS to induce LTP in the dHPC SC pathway, which plays a critical role in short-term spatial memory (72), in slices obtained from female mice in metestrus. Baseline slice recordings prior to LTP induction indicated no changes in basal synaptic function due to CNIH3 on maximal EPSP slope or paired pulse ratios (PPR) (Table S2). We observed no changes in the initial EPSP potentiation following the induction of LTP by HFS (Figure 6H), which aligned with our biochemical data indicating no differences in GluA1 expression (Figure 6B – C), as the rapid insertion of GluA1-containing AMPARs contribute to early phase LTP potentiation (52, 67). 60 min post-HFS, the maintenance of LTP was disrupted in the dHPC of *Cnih3*$^{-/-}$ female mice in metestrus compared to *Cnih3*$^{+/+}$ females in metestrus (Figure 6H – I). We next examined whether LTP can be induced under conditions that promoted greater degrees of synaptic activation to promote LTP maintenance (73). For these studies we induced LTP through TBS of slices submerged in a bath solution of ACSF containing an elevated Ca^{2+}/Mg^{2+} ratio to enhance Ca^{2+} influx (74, 75). 60 min following TBS-induction of LTP, no difference in LTP expression was observed between genotypes (Figures 6J – K). This experiment demonstrated that CNIH3 plays an important role in the maintenance of LTP in the dorsal hippocampus in female mice during metestrus, and that despite this deficit, stronger induction protocols can compensate for CNIH3-dependent weakening of LTP.

DISCUSSION

Learning and memory play a pivotal role in animal behavior, and dysregulation of the memory mechanisms are found in a wide array of psychiatric disorders. In this study, overexpression of *Cnih3* in the dHPC improved short-term spatial memory only in female mice, whereas short-term spatial memory was attenuated only in female *Cnih3*$^{-/-}$ mice. Impairments in spatial memory of female *Cnih3*$^{-/-}$ mice were particularly apparent during metestrus, a stage characterized by low circulating levels of β-estradiol and progesterone (59, 76). In the dHPC, a region which plays a key role in spatial learning and memory, we observed striking reductions in synaptic connectivity, changes in AMPAR subunit composition favoring GluA2-containing, Ca^{2+}-impermeable AMPAR configurations, and attenuation of HFS-induced LTP in the SC pathway. We hypothesize that AMPAR dysregulation results in deficits in synaptic connectivity and synaptic plasticity to attenuate short-term memory in female *Cnih3*$^{-/-}$ mice during metestrus (Figure 7).

One important consideration for this study is the potential role of CNIH3 outside of the nervous system on our sex-specific findings. Outside of the brain, CNIH3 is predominantly located in the pancreas, testis, ovaries, and uterus (77). In addition, CNIH proteins are involved in growth factor trafficking during development and in ER secretory pathway vesicular trafficking (78, 79). We demonstrated that viral overexpression of *Cnih3* in the dHPC improved spatial memory in female animals, but our global KO of *Cnih3* raises the possibility that CNIH3-mediated developmental disruption or hormonal dysregulation may contribute to attenuated memory in female *Cnih3*$^{-/-}$ mice. Future studies utilizing a conditional KO would be necessary to conclusively determine the necessity of CNIH3 in the dHPC on spatial memory in females.

Interestingly, we did not observe any changes in long-term spatial memory across sex, genotype, or estrous cycle stage. Prior studies suggest that long and short-term memory are regulated by distinct mechanisms across multiple brain regions (such as the hippocampus, parietal and entorhinal cortices, amygdala, and prefrontal cortex) (80). In our biochemical data, we found regional differences in the role of CNIH3 on AMPAR subunit composition between the dHPC and vHPC. We also did not observe changes in LTP following a stronger induction stimulus, TBS. This capability to rescue LTP expression with a more intense LTP induction may also enable CNIH3-independent mechanisms for the encoding of memories for extended storage. Therefore, we suggest that while CNIH3 plays a critical role for short-term memory retrieval in female animals, the storage and retrieval of long-term memory does not rely on CNIH3 but instead engages wider neural circuitry and alternative mechanisms.

The observance of sex differences in rodent behavior are highly dependent upon species, age, strain, stress, and memory task (81, 82). Due to the variability inherent to individual study designs, researchers have reported data ranging from sex differences in spatial memory ability (83), search strategies but not end-of-task performance (84), spatial memory retention but not short-term memory consolidation (85), or no overall observable sex differences (86, 87). Our study did not find any differences in spatial memory in the Barnes maze between WT male and female mice, suggesting that spatial memory may act through CNIH3-independent mechanisms in males.

Several reports have provided key insights into sexual dimorphism in AMPAR-associated mechanisms such as evoked LTP magnitude, AMPAR expression and AMPAR/NMDAR signaling in hippocampal synapses (83, 85, 87 – 89). The post-synaptic protein SynGAP interacts differentially with AMPAR-associated TARPs by sex (90), but further investigation is needed to determine how AMPARs and their auxiliary proteins mediate sexual dimorphism in spatial memory and glutamatergic mechanisms.

In female animals, the estrous cycle and sex hormones play key roles in memory and hippocampal function (81, 91–96). However, prior studies investigating the role of the estrous cycle on memory are mixed (97–100), and our study only found differences in spatial memory due to estrous cycling in *Cnih3*$^{-/-}$ females. Hippocampal glutamatergic activity, LTP, dendritic spine density, AM PAR surface diffusion, and AM PAR subunit stoichiometry have been reported to fluctuate during the estrous cycle and in the presence of 17β-estradiol (57, 58, 101–105). We hypothesize that CNIH3 masks estrous-specific deficits in hippocampal and AM PAR function, which are only revealed in the absence of CNIH3. Overall, the results obtained in our study add to the body of evidence that the estrous cycle and glutamatergic mechanisms interact to facilitate synaptic plasticity and memory in female animals.

Supplementary Material

Refer to Web version on PubMed Central for supplementary material.

ACKNOWLEDGEMENTS

This work was funded by grants from the National Institutes of Health (NIH), grant numbers DA041781 (J.A.M.), DA042581 (J.A.M.), DA042499 (J.A.M.), DA041883 (J.A.M., E.C.N., J.D.D.), DA045463 (J.A.M.), DA046436 (E.C.N), DA042620 (E.C.N.), NS094760 (T.T.K), and GM008151 (Washington University, H.E.F.). In addition, this work was also funded by grants from the BrightFocus Foundation (T.T.K.), the Brain Research Foundation (T.T.K.), and the McDonnell Center for Cellular and Molecular Neurobioloby (T.T.K). Experiments utilizing the Zeiss LSM 880 Confocal with Airyscan and Zeiss AxioScan Z1 microscopes and image analyses utilizing Bitplane Imaris 3D visualization software were performed through the use of the Washington University Center for Cellular Imaging (WUCCI) supported by Washington University School of Medicine, The Children's Discovery Institute of Washington University and St. Louis Children's Hospital (CDI-CORE-2015-505 and CDI-CORE-2019-813) and the Foundation for Barnes-Jewish Hospital (3770 and 4642). Viral vector packaging was performed by the Hope Center Viral Core at Washington University in St. Louis. The authors would also like to thank Susan Maloney, Ph.D., Rebecca Ouwenga, Ph.D., Carla Yuede, Ph.D., Nicolas Massaly, Ph.D., Grace Yuan, Krishna Vaidyanathan, Tania Lintz, Tamara Markovic, Justine Mae, Azra Zee, and Justin Meyer for technical assistance. A preprint of an early form of this manuscript was previously uploaded to bioRxiv: Frye, H. E. et al. Cornichon Homolog-3 (CNIH3) Modulates Spatial Memory in Female Mice. *bioRxiv*, 724104, doi:10.1101/724104 (2019).

REFERENCES

1. Cheng J, Dong J, Cui Y, Wang L, Wu B, Zhang C (2012): Interacting partners of AMPA-type glutamate receptors. J Mol Neurosci. 48:441–447. [PubMed: 22361832]
2. Haering SC, Tapken D, Pahl S, Hollmann M (2014): Auxiliary subunits: shepherding AMPA receptors to the plasma membrane. Membranes (Basel). 4:469–490. [PubMed: 25110960]
3. Jacobi E, von Engelhardt J (2017): Diversity in AMPA receptor complexes in the brain. Curr Opin Neurobiol. 45:32–38. [PubMed: 28376410]
4. Schwenk J, Baehrens D, Haupt A, Bildl W, Boudkkazi S, Roeper J, et al. (2014): Regional diversity and developmental dynamics of the AMPA-receptor proteome in the mammalian brain. Neuron. 84:41–54. [PubMed: 25242221]
5. Herring BE, Shi Y, Suh YH, Zheng CY, Blankenship SM, Roche KW, et al. (2013): Cornichon proteins determine the subunit composition of synaptic AMPA receptors. Neuron. 77:1083–1096. [PubMed: 23522044]
6. Schwenk J, Harmel N, Zolles G, Bildl W, Kulik A, Heimrich B, et al. (2009): Functional proteomics identify cornichon proteins as auxiliary subunits of AMPA receptors. Science. 323:1313–1319. [PubMed: 19265014]
7. Shanks NF, Cais O, Maruo T, Savas JN, Zaika EI, Azumaya CM, et al. (2014): Molecular dissection of the interaction between the AMPA receptor and cornichon homolog-3. J Neurosci. 34:12104–12120. [PubMed: 25186755]
8. Brown P, McGuire H, Bowie D (2018): Stargazin and cornichon-3 relieve polyamine block of AMPA receptors by enhancing blocker permeation. J Gen Physiol. 150:67–82. [PubMed: 29222130]
9. Nakagawa T (2019): Structures of the AMPA receptor in complex with its auxiliary subunit cornichon. Science. 366:1259–1263. [PubMed: 31806817]
10. Brockie PJ, Jensen M, Mellem JE, Jensen E, Yamasaki T, Wang R, et al. (2013): Cornichons control ER export of AMPA receptors to regulate synaptic excitability. Neuron. 80:129–142. [PubMed: 24094107]
11. Shi Y, Suh YH, Milstein AD, Isozaki K, Schmid SM, Roche KW, et al. (2010): Functional comparison of the effects of TARPs and cornichons on AMPA receptor trafficking and gating. Proc Natl Acad Sci U S A. 107:16315–16319. [PubMed: 20805473]
12. Harmel N, Cokic B, Zolles G, Berkefeld H, Mauric V, Fakler B, et al. (2012): AMPA receptors commandeer an ancient cargo exporter for use as an auxiliary subunit for signaling. PLoS One. 7:e30681. [PubMed: 22292017]
13. Coombs ID, Soto D, Zonouzi M, Renzi M, Shelley C, Farrant M, et al. (2012): Cornichons modify channel properties of recombinant and glial AMPA receptors. J Neurosci. 32:9796–9804. [PubMed: 22815494]

14. Kato AS, Gill MB, Ho MT, Yu H, Tu Y, Siuda ER, et al. (2010): Hippocampal AMPA receptor gating controlled by both TARP and cornichon proteins. Neuron. 68:1082–1096. [PubMed: 21172611]
15. Gill MB, Kato AS, Roberts MF, Yu H, Wang H, Tomita S, et al. (2011): Cornichon-2 modulates AMPA receptor-transmembrane AMPA receptor regulatory protein assembly to dictate gating and pharmacology. J Neurosci. 31:6928–6938. [PubMed: 21543622]
16. Hawken NM, Zaika EI, Nakagawa T (2017): Engineering defined membrane-embedded elements of AMPA receptor induces opposing gating modulation by cornichon 3 and stargazin. J Physiol. 595:6517–6539. [PubMed: 28815591]
17. Boudkkazi S, Brechet A, Schwenk J, Fakler B (2014): Cornichon2 dictates the time course of excitatory transmission at individual hippocampal synapses. Neuron. 82:848–858. [PubMed: 24853943]
18. Mauric V, Mölders A, Harmel N, Heimrich B, Sergeeva OA, Klöcker N (2013): Ontogeny repeats the phylogenetic recruitment of the cargo exporter cornichon into AMPA receptor signaling complexes. Mol Cell Neurosci. 56:10–17. [PubMed: 23403072]
19. Lein ES, Hawrylycz MJ, Ao N, Ayres M, Bensinger A, Bernard A, et al. (2007): Genome-wide atlas of gene expression in the adult mouse brain. Nature. 445:168–176. [PubMed: 17151600]
20. Oberlander JG, Woolley CS (2016): 17β-Estradiol Acutely Potentiates Glutamatergic Synaptic Transmission in the Hippocampus through Distinct Mechanisms in Males and Females. J Neurosci. 36:2677–2690. [PubMed: 26937008]
21. Clayton JA (2018): Applying the new SABV (sex as a biological variable) policy to research and clinical care. Physiol Behav. 187:2–5. [PubMed: 28823546]
22. Ben-Yaacov A, Gillor M, Haham T, Parsai A, Qneibi M, Stern-Bach Y (2017): Molecular Mechanism of AMPA Receptor Modulation by TARP/Stargazin. Neuron. 93:1126–1137.e1124. [PubMed: 28238551]
23. von Engelhardt J, Mack V, Sprengel R, Kavenstock N, Li KW, Stern-Bach Y, et al. (2010): CKAMP44: a brain-specific protein attenuating short-term synaptic plasticity in the dentate gyrus. Science. 327:1518–1522. [PubMed: 20185686]
24. Schwenk J, Harmel N, Brechet A, Zolles G, Berkefeld H, Müller CS, et al. (2012): High-resolution proteomics unravel architecture and molecular diversity of native AMPA receptor complexes. Neuron. 74:621–633. [PubMed: 22632720]
25. Shanks NF, Savas JN, Maruo T, Cais O, Hirao A, Oe S, et al. (2012): Differences in AMPA and kainate receptor interactomes facilitate identification of AMPA receptor auxiliary subunit GSG1L. Cell Rep. 1:590–598. [PubMed: 22813734]
26. Greger IH, Watson JF, Cull-Candy SG (2017): Structural and Functional Architecture of AMPA-Type Glutamate Receptors and Their Auxiliary Proteins. Neuron. 94:713–730. [PubMed: 28521126]
27. Kamalova A, Nakagawa T (2020): AMPA receptor structure and auxiliary subunits. J Physiol.
28. Khan Z, Carey J, Park HJ, Lehar M, Lasker D, Jinnah HA (2004): Abnormal motor behavior and vestibular dysfunction in the stargazer mouse mutant. Neuroscience. 127:785–796. [PubMed: 15283975]
29. Tao F, Skinner J, Su Q, Johns RA (2006): New role for spinal Stargazin in alpha-amino-3-hydroxy-5-methyl-4-isoxazolepropionic acid receptor-mediated pain sensitization after inflammation. J Neurosci Res. 84:867–873. [PubMed: 16791853]
30. Kim S, Thompson RF (2011): c-Fos, Arc, and stargazin expression in rat eyeblink conditioning. Behav Neurosci. 125:117–123. [PubMed: 21319893]
31. Okvist A, Fagergren P, Whittard J, Garcia-Osta A, Drakenberg K, Horvath MC, et al. (2011): Dysregulated postsynaptic density and endocytic zone in the amygdala of human heroin and cocaine abusers. Biol Psychiatry. 69:245–252. [PubMed: 21126734]
32. Xia Y, Portugal GS, Fakira AK, Melyan Z, Neve R, Lee HT, et al. (2011): Hippocampal GluA1-containing AMPA receptors mediate context-dependent sensitization to morphine. J Neurosci. 31:16279–16291. [PubMed: 22072679]

33. Wang Z, Yuan Y, Xie K, Tang X, Zhang L, Ao J, et al. (2016): PICK1 Regulates the Expression and Trafficking of AMPA Receptors in Remifentanil-Induced Hyperalgesia. Anesth Analg. 123:771–781. [PubMed: 27537764]
34. Mejias R, Adamczyk A, Anggono V, Niranjan T, Thomas GM, Sharma K, et al. (2011): Gain-of-function glutamate receptor interacting protein 1 variants alter GluA2 recycling and surface distribution in patients with autism. Proc Natl Acad Sci U S A. 108:4920–4925. [PubMed: 21383172]
35. Kessels HW, Malinow R (2009): Synaptic AMPA Receptor Plasticity and Behavior. Neuron. 61:340–350. [PubMed: 19217372]
36. Drummond JB, Simmons M, Haroutunian V, Meador-Woodruff JH (2012): Upregulation of cornichon transcripts in the dorsolateral prefrontal cortex in schizophrenia. Neuroreport. 23:1031–1034. [PubMed: 23103966]
37. Floor K, Barøy T, Misceo D, Kanavin OJ, Fannemel M, Frengen E (2012): A 1 Mb de novo deletion within 11q13.1q13.2 in a boy with mild intellectual disability and minor dysmorphic features. Eur J Med Genet. 55:695–699. [PubMed: 22986108]
38. Nelson EC, Agrawal A, Heath AC, Bogdan R, Sherva R, Zhang B, et al. (2016): Evidence of CNIH3 involvement in opioid dependence. Mol Psychiatry. 21:608–614. [PubMed: 26239289]
39. Billa SK, Sinha N, Rudrabhatla SR, Moron JA (2009): Extinction of morphine-dependent conditioned behavior is associated with increased phosphorylation of the GluR1 subunit of AMPA receptors at hippocampal synapses. Eur J Neurosci. 29:55–64. [PubMed: 19077125]
40. Billa SK, Liu J, Bjorklund NL, Sinha N, Fu Y, Shinnick-Gallagher P, et al. (2010): Increased insertion of glutamate receptor 2-lacking alpha-amino-3-hydroxy-5-methyl-4-isoxazole propionic acid (AMPA) receptors at hippocampal synapses upon repeated morphine administration. Mol Pharmacol. 77:874–883. [PubMed: 20159947]
41. Portugal GS, Al-Hasani R, Fakira AK, Gonzalez-Romero JL, Melyan Z, McCall JG, et al. (2014): Hippocampal long-term potentiation is disrupted during expression and extinction but is restored after reinstatement of morphine place preference. J Neurosci. 34:527–538. [PubMed: 24403152]
42. Fakira AK, Massaly N, Cohensedgh O, Berman A, Moron JA (2016): Morphine-Associated Contextual Cues Induce Structural Plasticity in Hippocampal CA1 Pyramidal Neurons. Neuropsychopharmacology. 41:2668–2678. [PubMed: 27170097]
43. Williams SB, Arriaga M, Post WW, Korgaonkar AA, Moron JA, Han EB (2019): Hippocampal Activity Dynamics During Contextual Reward Association in Virtual Reality Place Conditioning. bioRxiv. 545608.
44. West DB, Pasumarthi RK, Baridon B, Djan E, Trainor A, Griffey SM, et al. (2015): A lacZ reporter gene expression atlas for 313 adult KOMP mutant mouse lines. Genome Res. 25:598–607. [PubMed: 25591789]
45. Trifonov S, Yamashita Y, Kase M, Maruyama M, Sugimoto T (2016): Overview and assessment of the histochemical methods and reagents for the detection of β-galactosidase activity in transgenic animals. Anat Sci Int. 91:56–67. [PubMed: 26394634]
46. Morón JA, Brockington A, Wise RA, Rocha BA, Hope BT (2002): Dopamine uptake through the norepinephrine transporter in brain regions with low levels of the dopamine transporter: evidence from knock-out mouse lines. J Neurosci. 22:389–395. [PubMed: 11784783]
47. Morón JA, Abul-Husn NS, Rozenfeld R, Dolios G, Wang R, Devi LA (2007): Morphine administration alters the profile of hippocampal postsynaptic density-associated proteins: a proteomics study focusing on endocytic proteins. Mol Cell Proteomics. 6:29–42. [PubMed: 17028301]
48. Sauerbeck AD, Gangolli M, Reitz SJ, Salyards MH, Kim SH, Hemingway C, et al. (2020): SEQUIN Multiscale Imaging of Mammalian Central Synapses Reveals Loss of Synaptic Connectivity Resulting from Diffuse Traumatic Brain Injury. Neuron. 107:257–273. [PubMed: 32392471]
49. Reitz SJ, Sauerbeck AD, Kummer TT (2021): SEQUIN: An imaging and analysis platform for quantification and characterization of synaptic structures in mouse. STAR Protoc. 2:100268. [PubMed: 33490984]

50. Izumi Y, Zorumski CF (2019): Temperoammonic Stimulation Depotentiates Schaffer Collateral LTP via p38 MAPK Downstream of Adenosine A1 Receptors. J Neurosci. 39:1783–1792. [PubMed: 30622168]
51. IMPC (2016): Cnih3tm1a(KOMP)Wtsi. In: Consortium IMP, editor.
52. Lee HK, Takamiya K, Han JS, Man H, Kim CH, Rumbaugh G, et al. (2003): Phosphorylation of the AMPA receptor GluR1 subunit is required for synaptic plasticity and retention of spatial memory. Cell. 112:631–643. [PubMed: 12628184]
53. Matsuo N, Reijmers L, Mayford M (2008): Spine-type-specific recruitment of newly synthesized AMPA receptors with learning. Science. 319:1104–1107. [PubMed: 18292343]
54. Gandhi RM, Kogan CS, Messier C, Macleod LS (2014): Visual-spatial learning impairments are associated with hippocampal PSD-95 protein dysregulation in a mouse model of fragile X syndrome. Neuroreport. 25:255–261. [PubMed: 24323121]
55. Li J, Han Z, Cao B, Cai CY, Lin YH, Li F, et al. (2017): Disrupting nNOS-PSD-95 coupling in the hippocampal dentate gyrus promotes extinction memory retrieval. Biochem Biophys Res Commun. 493:862–868. [PubMed: 28888982]
56. Volk L, Kim C-H, Takamiya K, Yu Y, Huganir RL (2010): Developmental regulation of protein interacting with C kinase 1 (PICK1) function in hippocampal synaptic plasticity and learning. Proc Natl Acad Sci U S A. 107:21784–21789. [PubMed: 21106762]
57. Tada H, Koide M, Ara W, Shibata Y, Funabashi T, Suyama K, et al. (2015): Estrous Cycle-Dependent Phasic Changes in the Stoichiometry of Hippocampal Synaptic AMPA Receptors in Rats. PLoS One. 10:e0131359. [PubMed: 26121335]
58. Palomero-Gallagher N, Bidmon HJ, Zilles K (2003): AMPA, kainate, and NMDA receptor densities in the hippocampus of untreated male rats and females in estrus and diestrus. J Comp Neurol. 459:468–474. [PubMed: 12687711]
59. McLean AC, Valenzuela N, Fai S, Bennett SAL (2012): Performing vaginal lavage, crystal violet staining, and vaginal cytological evaluation for mouse estrous cycle staging identification. Journal of visualized experiments : JoVE.e4389–e4389. [PubMed: 23007862]
60. Cho KO, Hunt CA, Kennedy MB (1992): The rat brain postsynaptic density fraction contains a homolog of the Drosophila discs-large tumor suppressor protein. Neuron. 9:929–942. [PubMed: 1419001]
61. Ehrlich I, Klein M, Rumpel S, Malinow R (2007): PSD-95 is required for activity-driven synapse stabilization. Proc Natl Acad Sci U S A. 104:4176–4181. [PubMed: 17360496]
62. Mateos JM, Lüthi A, Savic N, Stierli B, Streit P, Gähwiler BH, et al. (2007): Synaptic modifications at the CA3-CA1 synapse after chronic AMPA receptor blockade in rat hippocampal slices. J Physiol. 581:129–138. [PubMed: 17303644]
63. Sala C, Segal M (2014): Dendritic spines: the locus of structural and functional plasticity. Physiol Rev. 94:141–188. [PubMed: 24382885]
64. Maras PM, Molet J, Chen Y, Rice C, Ji SG, Solodkin A, et al. (2014): Preferential loss of dorsal-hippocampus synapses underlies memory impairments provoked by short, multimodal stress. Mol Psychiatry. 19:811–822. [PubMed: 24589888]
65. Gerth F, Jäpel M, Pechstein A, Kochlamazashvili G, Lehmann M, Puchkov D, et al. (2017): Intersectin associates with synapsin and regulates its nanoscale localization and function. Proc Natl Acad Sci U S A. 114:12057–12062. [PubMed: 29078407]
66. Hruska M, Henderson NT, Xia NL, Le Marchand SJ, Dalva MB (2015): Anchoring and synaptic stability of PSD-95 is driven by ephrin-B3. Nat Neurosci. 18:1594–1605. [PubMed: 26479588]
67. Lee HK, Barbarosie M, Kameyama K, Bear MF, Huganir RL (2000): Regulation of distinct AMPA receptor phosphorylation sites during bidirectional synaptic plasticity. Nature. 405:955–959. [PubMed: 10879537]
68. Ehlers MD (2000): Reinsertion or degradation of AMPA receptors determined by activity-dependent endocytic sorting. Neuron. 28:511–525. [PubMed: 11144360]
69. Hayashi T, Huganir RL (2004): Tyrosine phosphorylation and regulation of the AMPA receptor by SRC family tyrosine kinases. J Neurosci. 24:6152–6160. [PubMed: 15240807]

70. Bannerman D, Grubb M, Deacon R, Yee B, Feldon J, Rawlins J (2003): Ventral hippocampal lesions affect anxiety but not spatial learning. Behavioural brain research. 139: 197–213. [PubMed: 12642189]
71. Moser E, Moser M, Andersen P (1993): Spatial learning impairment parallels the magnitude of dorsal hippocampal lesions, but is hardly present following ventral lesions. The Journal of Neuroscience. 13:3916–3925. [PubMed: 8366351]
72. Debanne D, Gähwiler BH, Thompson SM (1996): Cooperative interactions in the induction of long-term potentiation and depression of synaptic excitation between hippocampal CA3-CA1 cell pairs in vitro. Proc Natl Acad Sci U S A. 93:11225–11230. [PubMed: 8855337]
73. Morgan SL, Teyler TJ (2001): Electrical stimuli patterned after the theta-rhythm induce multiple forms of LTP. J Neurophysiol. 86:1289–1296. [PubMed: 11535677]
74. Larson J, Lynch G (1988): Role of N-methyl-D-aspartate receptors in the induction of synaptic potentiation by burst stimulation patterned after the hippocampal theta-rhythm. Brain Res. 441:111–118. [PubMed: 2896049]
75. Larson J, Munkácsy E (2015): Theta-burst LTP. Brain Res. 1621:38–50. [PubMed: 25452022]
76. Walmer DK, Wrona MA, Hughes CL, Nelson KG (1992): Lactoferrin expression in the mouse reproductive tract during the natural estrous cycle: correlation with circulating estradiol and progesterone. Endocrinology. 131:1458–1466. [PubMed: 1505477]
77. Uhlén M, Fagerberg L, Hallström BM, Lindskog C, Oksvold P, Mardinoglu A, et al. (2015): Proteomics. Tissue-based map of the human proteome. Science. 347:1260419. [PubMed: 25613900]
78. Roth S, Neuman-Silberberg FS, Barcelo G, Schüpbach T (1995): cornichon and the EGF receptor signaling process are necessary for both anterior-posterior and dorsal-ventral pattern formation in Drosophila. Cell. 81:967–978. [PubMed: 7540118]
79. Zhang P, Schekman R (2016): Distinct stages in the recognition, sorting and packaging of proTGFα into COPII coated transport vesicles. Mol Biol Cell. 27:1938–1947. [PubMed: 27122606]
80. Izquierdo I, Medina JH, Vianna MR, Izquierdo LA, Barros DM (1999): Separate mechanisms for short- and long-term memory. Behav Brain Res. 103:1–11. [PubMed: 10475159]
81. Spencer JL, Waters EM, Romeo RD, Wood GE, Milner TA, McEwen BS (2008): Uncovering the mechanisms of estrogen effects on hippocampal function. Front Neuroendocrinol. 29:219–237. [PubMed: 18078984]
82. Koss WA, Frick KM (2017): Sex differences in hippocampal function. J Neurosci Res. 95:539–562. [PubMed: 27870401]
83. Monfort P, Gomez-Gimenez B, Llansola M, Felipo V (2015): Gender differences in spatial learning, synaptic activity, and long-term potentiation in the hippocampus in rats: molecular mechanisms. ACS Chem Neurosci. 6:1420–1427. [PubMed: 26098845]
84. Locklear MN, Kritzer MF (2014): Assessment of the effects of sex and sex hormones on spatial cognition in adult rats using the Barnes maze. Horm Behav. 66:298–308. [PubMed: 24937438]
85. Qi X, Zhang K, Xu T, Yamaki VN, Wei Z, Huang M, et al. (2016): Sex Differences in Long-Term Potentiation at Temporoammonic-CA1 Synapses: Potential Implications for Memory Consolidation. PLoS One. 11:e0165891. [PubMed: 27806108]
86. Frick KM, Burlingame LA, Arters JA, Berger-Sweeney J (1999): Reference memory, anxiety and estrous cyclicity in C57BL/6NIA mice are affected by age and sex. Neuroscience. 95:293–307.
87. Dachtler J, Fox KD, Good MA (2011): Gender specific requirement of GluR1 receptors in contextual conditioning but not spatial learning. Neurobiol Learn Mem. 96:461–467. [PubMed: 21810476]
88. Xiang X, Huang W, Haile CN, Kosten TA (2011): Hippocampal GluR1 associates with behavior in the elevated plus maze and shows sex differences. Behav Brain Res. 222:326–331. [PubMed: 21497621]
89. Moidunny S, Benneyworth MA, Titus DJ, Beurel E, Kolli U, Meints J, et al. (2020): Glycogen synthase kinase-3 inhibition rescues sex-dependent contextual fear memory deficit in human immunodeficiency virus-1 transgenic mice. Br J Pharmacol. 177:5658–5676. [PubMed: 33080056]

90. Mastro TL, Preza A, Basu S, Chattarji S, Till SM, Kind PC, et al. (2020): A sex difference in the response of the rodent postsynaptic density to synGAP haploinsufficiency. Elife. 9:e52656. [PubMed: 31939740]
91. Foy MR, Akopian G, Thompson RF (2008): Progesterone regulation of synaptic transmission and plasticity in rodent hippocampus. Learn Mem. 15:820–822. [PubMed: 18984562]
92. Woolley CS, Gould E, Frankfurt M, McEwen BS (1990): Naturally occurring fluctuation in dendritic spine density on adult hippocampal pyramidal neurons. J Neurosci. 10:4035–4039. [PubMed: 2269895]
93. Woolley CS, McEwen BS (1992): Estradiol mediates fluctuation in hippocampal synapse density during the estrous cycle in the adult rat. J Neurosci. 12:2549–2554. [PubMed: 1613547]
94. McEwen BS, Woolley CS (1994): Estradiol and progesterone regulate neuronal structure and synaptic connectivity in adult as well as developing brain. Exp Gerontol. 29:431–436. [PubMed: 7925761]
95. Woolley CS, Wenzel HJ, Schwartzkroin PA (1996): Estradiol increases the frequency of multiple synapse boutons in the hippocampal CA1 region of the adult female rat. J Comp Neurol. 373:108–117. [PubMed: 8876466]
96. Woolley CS (1998): Estrogen-mediated structural and functional synaptic plasticity in the female rat hippocampus. Horm Behav. 34:140–148. [PubMed: 9799624]
97. Frick KM, Berger-Sweeney J (2001): Spatial reference memory and neocortical neurochemistry vary with the estrous cycle in C57BL/6 mice. Behav Neurosci. 115:229–237. [PubMed: 11256446]
98. Cordeira J, Kolluru SS, Rosenblatt H, Kry J, Strecker RE, McCarley RW (2018): Learning and memory are impaired in the object recognition task during metestrus/diestrus and after sleep deprivation. Behavioural Brain Research. 339:124–129. [PubMed: 29180134]
99. Broestl L, Worden K, Moreno AJ, Davis EJ, Wang D, Garay B, et al. (2018): Ovarian Cycle Stages Modulate Alzheimer-Related Cognitive and Brain Network Alterations in Female Mice. eneuro. 5:ENEURO.0132-0117.2018.
100. Berry B, McMahan R, Gallagher M (1997): Spatial learning and memory at defined points of the estrous cycle: Effects on performance of a hippocampal-dependent task. Behavioral Neuroscience. 111:267–274. [PubMed: 9106667]
101. Woolley CS, McEwen BS (1994): Estradiol regulates hippocampal dendritic spine density via an N-methyl-D-aspartate receptor-dependent mechanism. J Neurosci. 14:7680–7687. [PubMed: 7996203]
102. Woolley CS, Weiland NG, McEwen BS, Schwartzkroin PA (1997): Estradiol increases the sensitivity of hippocampal CA1 pyramidal cells to NMDA receptor-mediated synaptic input: correlation with dendritic spine density. J Neurosci. 17:1848–1859. [PubMed: 9030643]
103. Foy MR, Xu J, Xie X, Brinton RD, Thompson RF, Berger TW (1999): 17beta-estradiol enhances NMDA receptor-mediated EPSPs and long-term potentiation. J Neurophysiol. 81:925–929. [PubMed: 10036289]
104. Bechard AR, Hamor PU, Schwendt M, Knackstedt LA (2018): The effects of ceftriaxone on cue-primed reinstatement of cocaine-seeking in male and female rats: estrous cycle effects on behavior and protein expression in the nucleus accumbens. Psychopharmacology (Berl). 235:837–848. [PubMed: 29197981]
105. Waters EM, Mitterling K, Spencer JL, Mazid S, McEwen BS, Milner TA (2009): Estrogen receptor alpha and beta specific agonists regulate expression of synaptic proteins in rat hippocampus. Brain Res. 1290:1–11. [PubMed: 19596275]

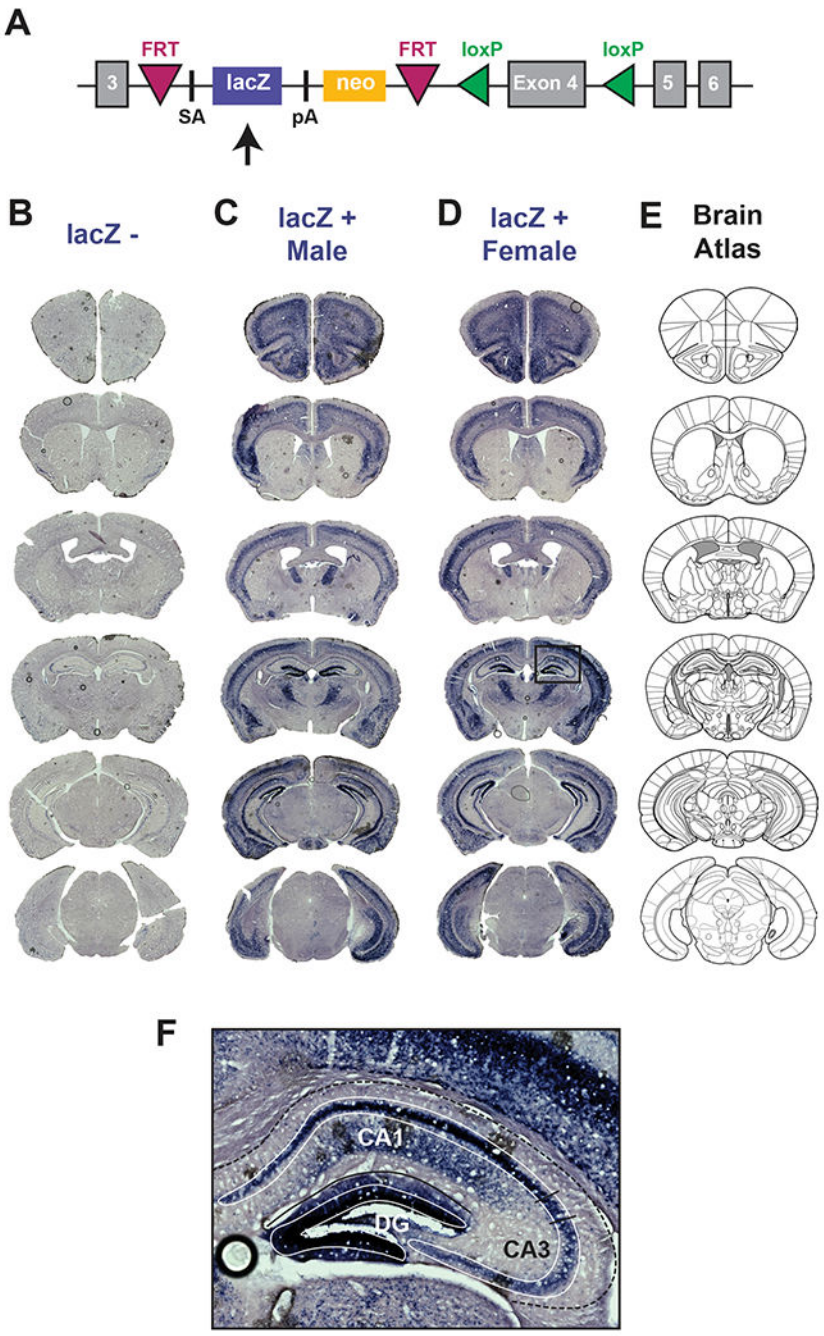

Figure 1: *LacZ*-tagged *Cnih3* prominently expressed in the CA1 and dentate gyrus regions of the hippocampus

(A) Using the *lacZ* cassette contained within the *Cnih3*$^{tm1a(KOMP)wtsi}$ gene, a β-galactosidase staining assay was used to identify regional *Cnih3* expression throughout the brain. (B – D) Representative slices from (B) lacZ− and from lacZ+ (C) male and (D) female brain slices are shown next to (E) corresponding illustrations. (E) A higher magnification image of a lacZ+ dHPC showed strong lacZ expression in the CA1 and dentate gyrus regions of the dHPC.

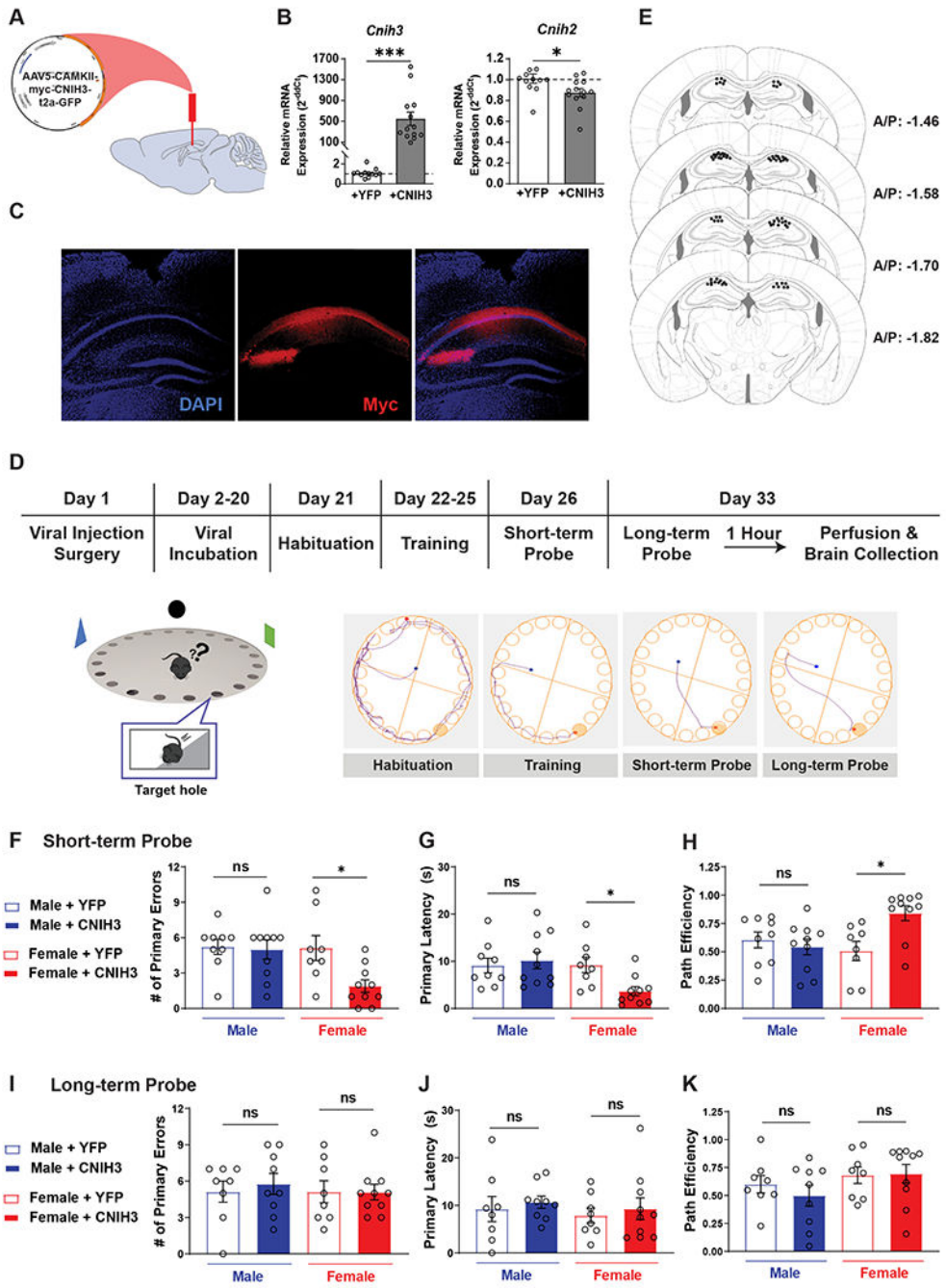

Figure 2: *Cnih3* overexpression in the dorsal hippocampus improved short-term memory in female mice

(A) AAV5-CAMKII-myc-CNIH3-t2a-GFP or AAV5-CAMKII-eYFP viruses were injected bilaterally into the dorsal hippocampus of WT male and female mice to overexpress *Cnih3* (−1.8 mm A/P, ±1.4 mm M/L, −1.8 mm D/V). (B) RT-qPCR results of the dorsal hippocampus for *Cnih3* and *Cnih2* mRNA 3 weeks following viral injection of YFP (n = 12) and *Cnih3* overexpression (n = 13) viruses. No differences due to sex were observed in *Cnih3* (*2-way ANOVA*, ***Sex**: $F_{(1, 21)} = 0.2947$, $p = 0.5929$*, ***Virus x Sex**: $F_{(1, 21)} =$

0.2939, p = 0.5934) or *Cnih2* expression (***Sex****: $F_{(1, 21)}$ = 0.5387, p = 0.4711*, ***Virus x Sex****: $F_{(1, 21)}$ = 0.5387, p = 0.4711*) in either group, therefore they were combined for statistical analysis. *(Two-tailed unpaired t test, Cnih3: p = 0.0005; Cnih2: p = 0.0301).* (C) Immunohistochemical representative image of a brain injected with AAV5-CAMKII-myc-CNIH3-t2a-GFP. Brain slices were probed for the myc-tag adjacent to *Cnih3* in the viral construct. (D) Timeline for injection of virus and Barnes Maze testing. (E) Injection placements for AAV5-CAMKII-myc-CNIH3-t2a-GFP and YFP AAV5-CAMKII-eYFP viruses of animals tested in the Barnes Maze. (F – H) Barnes Maze results of male and female mice injected with either YFP (male: n = 9; female: n = 8) or *Cnih3* overexpression (male: n = 10; female: n = 10) virus during the short-term probe trial represented by (F) primary errors before location of the target hole, (G) primary latency to entry into the target hole, and (H) path efficiency to the target hole. (*Two-way ANOVA*, **Sex:** *Primary errors: $F_{(1, 33)}$ = 4.362, p = 0.0445; Primary latency: $F_{(1, 33)}$ = 4.429, p = 0.0430; Path efficiency: $F_{(1, 33)}$ = 1.908, p = 0.1765*; **Virus**: *Primary errors: $F_{(1, 33)}$ = 5.071, p = 0.0311; Primary latency: $F_{(1, 33)}$ = 4.429, p = 0.1497; Path efficiency: $F_{(1, 33)}$ = 3.536, p = 0.0689*; **Sex x Virus:** *Primary errors: $F_{(1, 33)}$ = 3.848, p = 0.0583; Primary latency: $F_{(1, 33)}$ = 4.783, p = 0.0359; Path efficiency: $F_{(1, 33)}$ = 7.438, p = 0.0101*). (F) Primary errors (*post-hoc Sidak's multiple comparisons test, male YFP vs. CNIH3: p = 0.9731, female YFP vs. CNIH3: p = 0.0121, male YFP vs. female YFP: p > 0.9999)* (G) Primary Latency (*male YFP vs. CNIH3: p = 0.8497, female YFP vs. CNIH3: p = 0.0310, male YFP vs. female YFP: p > 0.9999*. (H) Path Efficiency (*male YFP vs. CNIH3: p = 0.7947, female YFP vs. CNIH3: p = 0.0059, male YFP vs. female YFP: p = 0.9356*) (I – K) Barnes Maze results from the long-term probe for (I) primary errors, (J) primary latency, and (K) path efficiency. (*Two-way ANOVA,* ***Sex:*** *Primary errors: $F_{(1, 31)}$ = 0.5714, p = 0.6817; Primary latency: $F_{(1, 31)}$ = 0.4544, p = 0.5053; Path efficiency: $F_{(1, 31)}$ = 2.674, p = 0.1121,* ***Virus:*** *Primary errors: $F_{(1, 31)}$ = 0.5714, p = 0.6817; Primary latency: $F_{(1, 31)}$ = 0.4966, p = 0.4863; Path efficiency: $F_{(1, 31)}$ = 0.2696, p = 0.6073,* ***Sex x Virus:*** *Primary errors: $F_{(1, 31)}$ = 0.5714, p = 0.6817; Primary latency: $F_{(1, 31)} = 4.18X10^{-5}$, p = 0.9949; Path efficiency: $F_{(1: 31)}$ = 0.4638, p = 0.5009).*

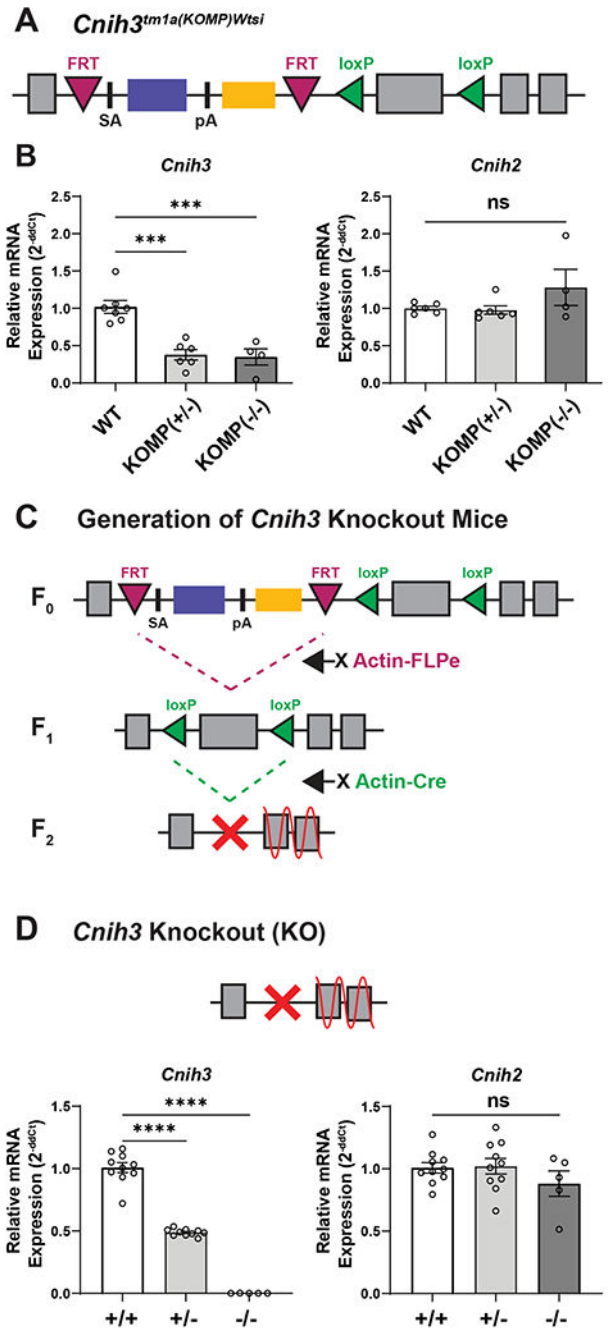

Figure 3: Generation and characterization of *Cnih3* knockout (KO) mice

(A) *Cnih3*$^{tm1a(KOMP)Wtsi}$ mice obtained from the Knockout Mouse Project (KOMP). The *Cnih3*$^{tm1a(KOMP)Wtsi}$ gene contained a polyadenylation (pA) site after exon 3 to halt mRNA transcription. The pA site as well as lacZ and neo cassettes and a splice acceptor (SA) site were contained within two FRT sites. Exon 4 was surrounded by two loxP sites. *Cnih3*$^{tm1a(KOMP)wtsi}$ mice were bred to create a colony of WT, heterozygote (KOMP(+/−)), and homozygote (KOMP(−/−)) *Cnih3*$^{tm1a(KOMP)wtsi}$ mice. RT-qPCR analysis was conducted to measure mRNA expression for Cnih3 and Cnih2 compared to WT controls. (B) RT-

qPCR results for WT (n = 7), KOMP(+/−) (n = 6), and KOMP(−/−) (n = 4) mice for expression of *Cnih3* and *Cnih2* mRNA. Relative mRNA expression presented using ddCt analysis. Ct values were normalized to β-actin loading controls and then to the average of β-actin-normalized WT values. Relative mRNA expression presented as relative fold change calculated by $2^{-(ddCt)}$. (*Cnih3: one-way ANOVA,* $F_{(2, 14)} = 20.40$, $p < 0.0001$, *post-hoc Sidak's multiple comparisons test,* $p = 0.0001$ *and 0.0003 respectively. Cnih2:* $F_{(2, 13)} = 2.041$, $p = 0.1695$) (C) Breeding scheme for *Cnih3* KO mice from $Cnih3^{tm1a(KOMP)wtsi}$ mice. $Cnih3^{tm1a(KOMP)wtsi}$ male mice (F0) were bred with Actin-FLPe females to excise cassettes between the FRT sites. Male F1 mice were bred with Actin-Cre females to excise exon 4 contained within the loxP sites. Mice in generation F2 are $Cnih3^{+/-}$ which were bred to create a colony of $Cnih3^{+/+}$, $Cnih3^{+/-}$, and $Cnih3^{-/-}$ animals. (D) RT-qPCR results for *Cnih3* and *Cnih2* mRNA expression in $Cnih3^{+/+}$ (n = 10), $Cnih3^{+/-}$ (n = 10), and $Cnih3^{-/-}$ (n = 5) mice. Male and female mice did not show differences in gene expression for *Cnih3* (*2-way ANOVA,* ***Sex****:* $F_{(1, 19)} = 0.03087$, $p = 0.8624$, ***Genotype****:* $F_{(2, 19)} = 217.7$, $p < 0.0001$, ***Sex x Genotype****:* $F_{(2, 19)} = 0.01556$, $p = 0.9846$) or *Cnih2* expression (***Sex****:* $F_{(1, 19)} = 0.07662$, $p = 0.7849$, ***Genotype****:* $F_{(2, 19)} = 0.7778$, $p = 0.4735$, ***Sex x Genotype****:* $F_{(2, 19)} = 3.228$, $p = 0.0621$) in either group, therefore they were combined for statistical analysis. (*Cnih3:* $F_{(2, 22)} = 264.1$, $p < 0.0001$, *post-hoc Sidak's multiple comparisons test,* $p < 0.0001$ *each. Cnih2:* $F_{(2, 22)} = 1.097$, $p = 0.3513$).

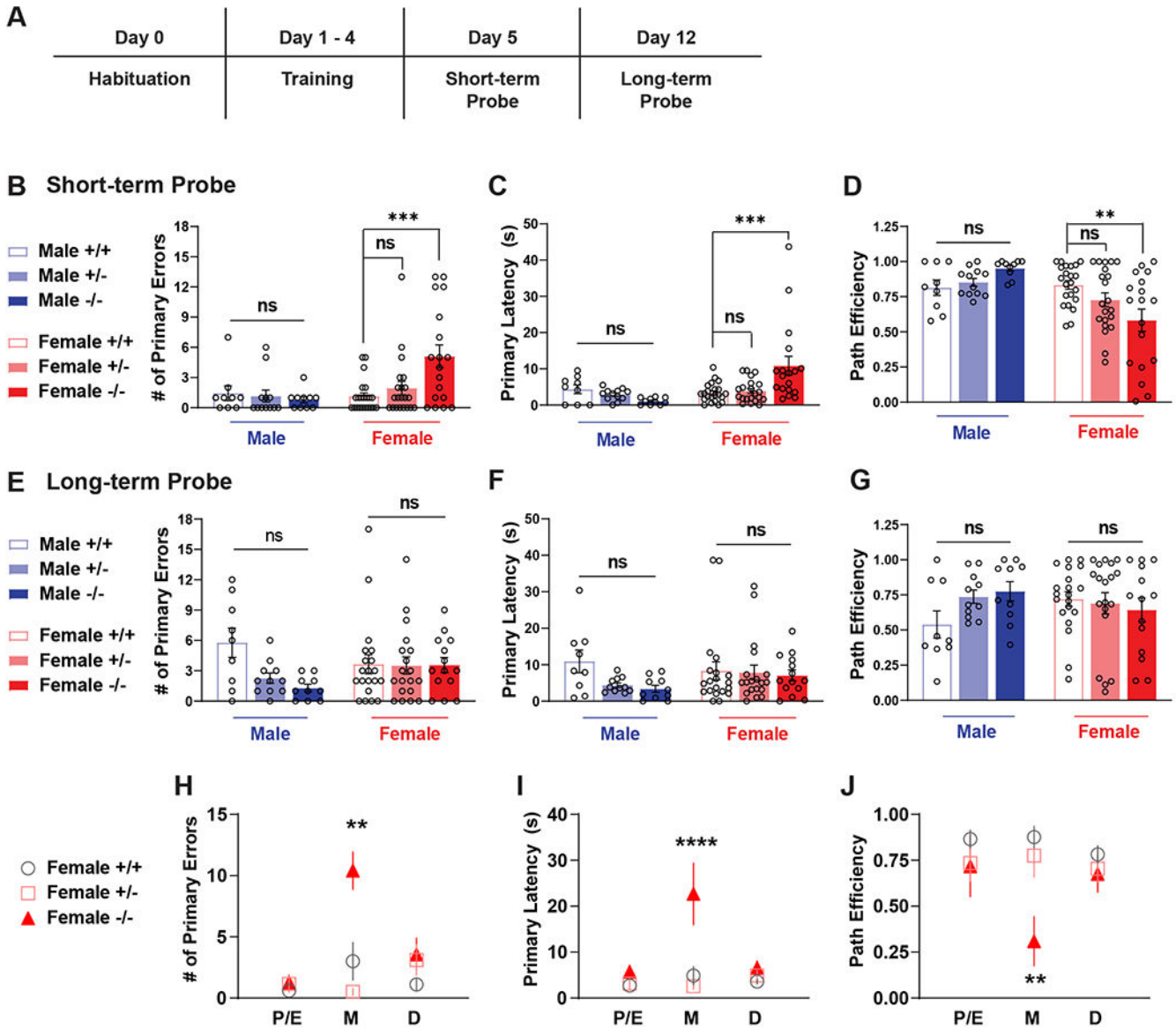

Figure 4: Short-term spatial memory impaired in female *Cnih3*$^{-/-}$ mice during metestrus

(A) Time course Barnes maze spatial memory paradigm. (B – D) Barnes Maze results of male and female *Cnih3*$^{+/+}$ (male: n = 9; female: n = 22), *Cnih3*$^{+/-}$ (male: n = 12; female: n = 21), and *Cnih3*$^{-/-}$ (male: n =10; female: n = 18) mice during the short-term probe trials represented by (B) primary errors before location of the target hole, (C) primary latency to entry into the target hole, and (D) path efficiency to the target hole. (*Two-way ANOVA,* ***Sex:*** *Primary errors:* $F_{(1, 86)} = 6.158$, $p = 0.015$; *Primary latency:* $F_{(1, 86)} = 7.338$, $p = 0.0081$; *Path efficiency:* $F_{(1, 86)} = 11.71$, $p = 0.001$, ***Genotype:*** *Primary errors:* $F_{(2, 86)} = 2.479$, $p = 0.0898$; *Primary latency:* $F_{(2, 86)} = 1.705$, $p = 0.1878$; *Path efficiency:* $F_{(2, 86)} = 0.4759$, $p = 0.623$, ***Sex x Genotype:*** *Primary errors:* $F_{(2, 86)} = 4.493$, $p = 0.0139$; *Primary latency:* $F_{(2, 86)} = 7.249$, $p = 0.0012$; *Path efficiency:* $F_{(2, 86)} = 5.704$, $p = 0.0047$). (B) Primary errors (*post-hoc Sidak's multiple comparisons test, male Cnih3*$^{+/+}$ *and Cnih3*$^{+/-}$ vs. *male Cnih3*$^{-/-}$: $p > 0.9999$ *each, female Cnih3*$^{+/+}$ *and Cnih3*$^{+/-}$ vs. *female Cnih3*$^{-/-}$: *p*

= 0.0006 & p = 0.0156 respectively, male Cnih3$^{+/+}$ vs. female Cnih3$^{+/+}$: p > 0.9999). (C) Primary latency (*male Cnih3$^{+/+}$ and Cnih3$^{+/-}$* vs. *male Cnih3$^{-/-}$: p = 0.9580 & p = 0.9998 respectively, female Cnih3$^{+/+}$ and Cnih3$^{+/-}$* vs. *female Cnih3$^{-/-}$: p = 0.0006 & p = 0.0021, male Cnih3$^{+/+}$ vs. female Cnih3$^{+/+}$: p > 0.9999*). (D) Path efficiency (*male Cnih3$^{+/+}$ and Cnih3$^{+/-}$* vs. *male Cnih3$^{-/-}$: p = 0.9188 & p = 0.9907 respectively, female Cnih3$^{+/+}$ and Cnih3$^{+/-}$* vs. *female Cnih3$^{-/-}$: p = 0.0043 & p = 0.3927, male Cnih3$^{+/+}$ vs. female Cnih3$^{+/+}$: p > 0.9999*). (E – G) Barnes Maze results of male and female *Cnih3$^{+/+}$* (male: n = 9; female: n = 20), *Cnih3$^{+/-}$* (male: n = 11, one animal froze during long-term probe and was therefore excluded; female: n = 19), and *Cnih3$^{-/-}$* (male: n =10; female: n = 14) mice which were also tested in long-term probe trials represented by (E) primary errors, (F) primary latency, and (G) path efficiency (some females were euthanized following the short-term trial for other experiments, thus were not tested in a long-term trial). (*Two-way ANOVA, **Sex**: Primary Errors: $F_{(1, 77)} = 0.3644$, p = 0.5479; Primary Latency: $F_{(1, 77)} = 0.6953$, p = 0.4070; Path Efficiency: $F_{(1, 77)} = 0.0001843$, p = 0.9892; **Genotype**: Primary Errors: $F_{(2, 77)} = 3.170$, p = 0.0475; Primary Latency: $F_{(2, 77)} = 2.097$, p = 0.1298; Path Efficiency: $F_{(2, 77)} = 0.4683$, p = 0.4683; **Sex x Genotype:** Primary Errors: $F_{(2, 77)} = 2.892$, p = 0.0615; Primary Latency: $F_{(2, 77)} = 1.253$, p = 0.2915; Path Efficiency: $F_{(2, 77)} = 2.194$, p = 0.1184; Primary errors post-hoc Sidak's multiple comparisons test, male Cnih3$^{+/+}$* vs. *male Cnih3$^{-/-}$: p = 0.0695*). (H – J) Female animals were subdivided into mice in the proestrus/estrus (P/E), metestrus (M), and diestrus. For sufficient group size, we combined data from mice in proestrus and estrus due to similarity in hormonal levels in these stages (59). (D) phases of the estrous cycle during the short-term probe trial in the Barnes Maze (Cnih3$^{+/+}$ total n = 22: proestrus/estrus n = 10, metestrus n = 3, diestrus n = 9; Cnih3$^{+/-}$ total n = 21: proestrus/estrus n = 7, metestrus n = 4, diestrus n = 10; Cnih3$^{-/-}$ total n = 18: proestrus/estrus n = 4, metestrus n = 5, diestrus n = 9). Data shown in these figures from individual mice are shown in Figure S5. Estrous cycle stage was correlated to animal performance in the short-term probe trial represented by (H) primary errors, (I) primary latency, and (J) path efficiency. (H – J) (*Two-way ANOVA, **Estrous cycle:** Primary errors: $F_{(2, 52)} = 6.443$, p = 0.0032; Primary latency: $F_{(2, 52)} = 5.442$, p = 0.0071; Path Efficiency: ($F_{(2, 52)} = 0.9325$, p = 0.4000) **Genotype:** Primary errors: $F_{(2, 52)} = 9.206$, p = 0.0004; Primary latency: $F_{(2, 52)} = 13.14$, p < 0.0001; Path Efficiency: $F_{(2, 52)} = 5.820$, p = 0.0052; **Estrous x Genotype:** Primary errors: $F_{(4, 52)} = 5.628$, p = 0.0008; Primary latency: $F_{(4, 52)} = 5.908$, p = 0.0005; Path Efficiency: $F_{(4, 52)} = 2.060$, p = 0.0995*). (H) Primary Errors: (*post-hoc Sidak's multiple comparisons test, metestrus Cnih3$^{+/+}$ and Cnih3$^{+/-}$ vs. metestrus Cnih3$^{-/-}$: p = 0.0013 & p < 0.0001, proestrus/estrus and diestrus vs. Cnih3$^{-/-}$ metestrus: p < 0.0001 each*). (I) Primary Latency: (*post-hoc Sidak's multiple comparisons test, metestrus Cnih3$^{+/+}$ and Cnih3$^{+/-}$ vs. metestrus Cnih3$^{-/-}$: p < 0.0001 each, proestrus/estrus and diestrus vs. Cnih3$^{-/-}$ metestrus: p < 0.0001 each*). (J) Path Efficiency: (*post-hoc Sidak's multiple comparisons test, metestrus Cnih3$^{+/+}$ and Cnih3$^{+/-}$ vs. metestrus Cnih3$^{-/-}$: p = 0.0045 & p = 0.0122, proestrus/estrus and diestrus vs. Cnih3$^{-/-}$ metestrus: p = 0.0224 & p = 0.0129).*

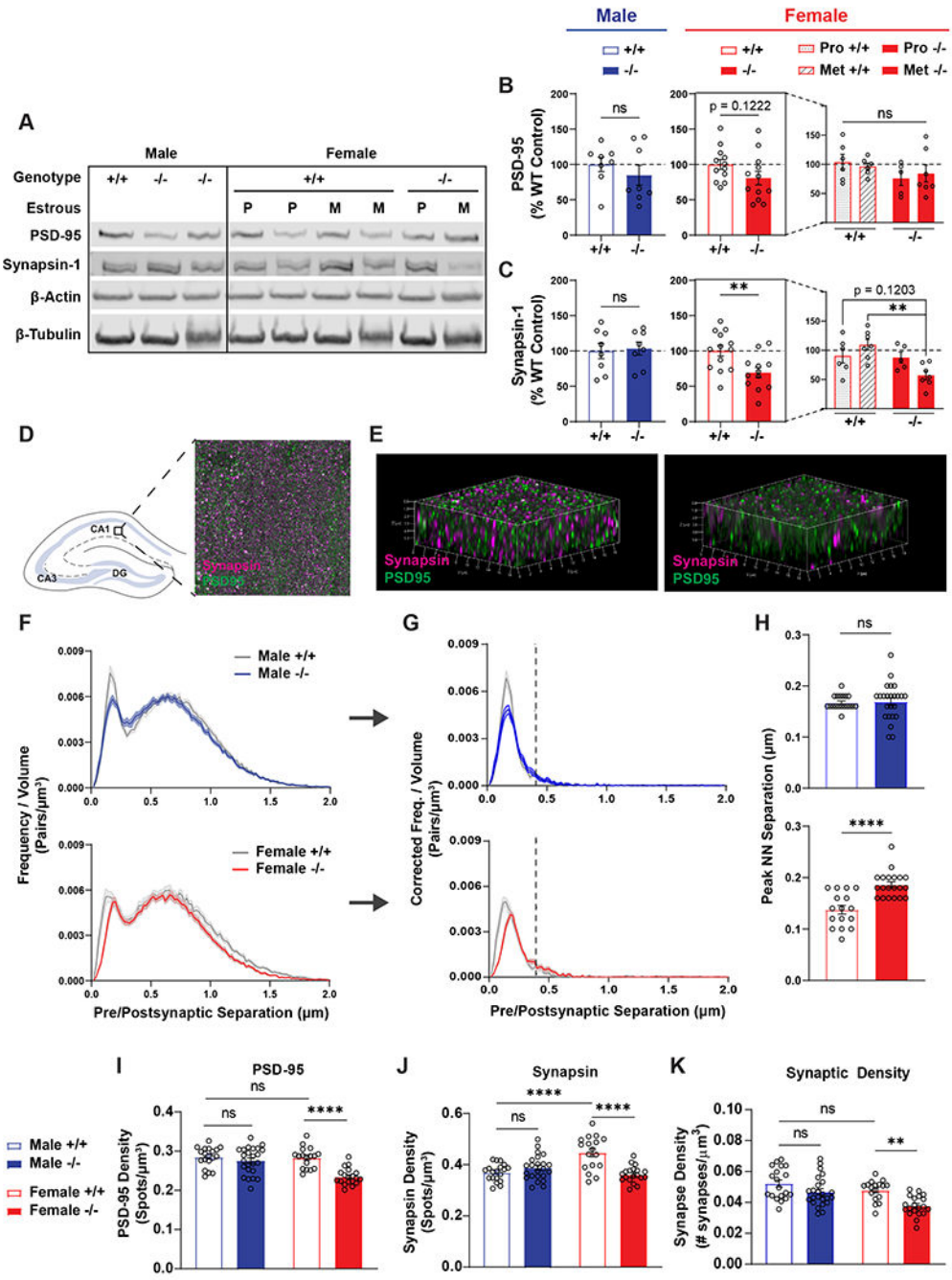

Figure 5: Reduced synaptic density and weakened synaptic connectivity in the dHPC of *Cnih3*$^{-/-}$ female mice

(A) Example western blot images from male and female *Cnih3*$^{+/+}$ (male: n = 8; female: n = 13) and *Cnih3*$^{-/-}$ (male: n = 8; female: n = 12) animals. Each lane represents dHPC whole-cell homogenate fractions obtained from a single animal. Female samples were collected during proestrus and metestrus stages for both *Cnih3*$^{+/+}$ (proestrus: n = 6; metestrus: n = 7) and *Cnih3*$^{-/-}$ (proestrus: n = 5; metestrus: n = 7) genotypes, these estrous cycle stages were selected based on the memory deficits we previously observed during metestrus, but not proestrus, in *Cnih3*$^{-/-}$ female mice (Figure 4) One sample was removed from the analysis

for both *Cnih3*$^{+/+}$ and *Cnih3*$^{-/-}$ proestrus female datasets due incorrect estrous cycle stage at the time of death. Blots were probed for PSD-95, Synapsin-1, and HKPs β-actin (used for normalization) and β-tubulin. Datasets were normalized to within-sex and within-blot *Cnih3*$^{+/+}$ controls, data is shown as normalized percentages to the baseline average of *Cnih3*$^{+/+}$ controls (set at 100%). (B) Quantification of PSD-95 within males (*Two-tailed unpaired t test, p = 0.4011)* and within females (*p = 0.1222) (if female Cnih3*$^{+/+}$ *normalized to male Cnih3*$^{+/+}$ *average: male Cnih3*$^{+/+}$ *vs. female Cnih3*$^{+/+}$ *p = 0.2627*). Female data was also subdivided by estrous cycle stage (*Two-way ANOVA,* ***Estrous Cycle****:* $F_{(1, 20)} = 0.001252, p = 0.9721$; ***Genotype:*** $F_{(1, 20)} = 2.538, p = 0.1268$; ***Estrous Cycle x Genotype****:* $F_{(1, 20)} = 0.4022, p = 0.5331$). (C) Quantification of synapsin-1 within males (*Two-tailed unpaired t test, p = 0.8086) and within females (p = 0.0077) (if female Cnih3*$^{+/+}$ *normalized to male Cnih3*$^{+/+}$ *average: male Cnih3*$^{+/+}$ *vs. female Cnih3*$^{+/+}$ *p = 0.8598).* Female data was also subdivided by estrous cycle (*Two-way ANOVA,* ***Estrous Cycle****:* $F_{(1, 21)} = 0.3485, p = 0.5613$; ***Genotype:*** $F_{(1, 21)} = 8.801, p = 0.0097$; ***Estrous Cycle x Genotype****:* $F_{(1, 21)} = 6.622, p = 0.0177$, *post-hoc Sidak's multiple comparisons test, metestrus Cnih3*$^{+/+}$ *vs. metestrus Cnih3*$^{-/-}$*: p = 0.0031, proestrus Cnih3*$^{+/+}$ *vs. metestrus Cnih3*$^{-/-}$*: p = 0.1203*). (D) SEQUIN multiscale imaging was utilized to quantify synaptic loci in the CA1 of the dorsal hippocampus. We chose to focus on the CA1 region of the dHPC for this experiment due to its critical role in spatial memory and its pronounced expression of *Cnih3* (Figure 1F). Fixed brain slices were stained for the synapsin and PSD95, imaged by super-resolution ISM with Airyscan, and images underwent 3D nearest neighbor analysis to identify synaptic loci (See Figure S10). (E) Representative 3D images of the CA1 region of the dHPC from *Cnih3*$^{+/+}$ (inset from panel D marked by *) and Cnih3$^{-/-}$ female mice. (F) Average frequency distributions of male and female pre- and postsynaptic pairs (n = 17 – 24 slices/group across n = 3 – 4 animals/group, description of relevant statistical outliers provided in Table S1), and (G) corrected frequency distribution obtained by subtraction of randomized pairs to isolate the early peak used to identify synaptic loci <400nm (dotted line). (H) Nearest neighbor (NN) separation distances of the synaptic peaks in panel G for males (*Two-tailed Mann-Whitney test, male Cnih3*$^{+/+}$ *vs. male Cnih3*$^{-/-}$*, p = 0.5778) and females (female Cnih3*$^{+/+}$ *vs. female Cnih3*$^{-/-}$*; p < 0.0001). (Male Cnih3*$^{+/+}$ *vs. female Cnih3*$^{+/+}$*: p = 0.00059* (I) Quantification of the top 20% of PSD-95 (*Two-way ANOVA,* ***Sex****:* $F_{(1, 75)} = 11.35, p = 0.0012$; ***Genotype:*** $F_{(1, 75)} = 21.09, p < 0.0001$; ***Sex x Genotype****:* $F_{(1, 75)} = 9.623, p = 0.0027$; *Post-hoc Sidak's multiple comparisons test, male Cnih3*$^{+/+}$ *vs. male Cnih3*$^{-/-}$*: p = 0.8542, female Cnih3*$^{+/+}$ *vs. female Cnih3*$^{-/-}$ *p < 0.0001, male Cnih3*$^{+/+}$ *vs. female Cnih3*$^{+/+}$ *p > 0.9999*) and (J) Synapsin puncta (*Two-way ANOVA,* ***Sex****:* $F_{(1, 74)} = 5.96, p = 0.0170$; ***Genotype:*** $F_{(1, 74)} = 9.753, p = 0.0026$; ***Sex x Genotype****:* $F_{(1, 74)} = 23.59, p < 0.0001$; *Post-hoc Sidak's multiple comparisons test, male Cnih3*$^{+/+}$ *vs. male Cnih3*$^{-/-}$*: p = 0.7507, female Cnih3*$^{+/+}$ *vs. female Cnih3*$^{-/-}$ *p < 0.0001, male Cnih3*$^{+/+}$ *vs. female Cnih3*$^{+/+}$ *p < 0.0001*). (K) Quantification of synaptic loci identified with SEQUIN (*Two-way ANOVA,* ***Sex****:* $F_{(1, 76)} = 12.45, p = 0.0007$; ***Genotype****:* $F_{(1, 76)} = 16.22, p = 0.0001$; ***Sex x Genotype****:* $F_{(1, 76)} = 1.515, p = 0.2222$; *Post-hoc Sidak's multiple comparisons test, male Cnih3*$^{+/+}$ *vs. male Cnih3*$^{-/-}$*: p = 0.2346, female Cnih3*$^{+/+}$ *vs. female Cnih3*$^{-/-}$ *p = 0.0035, male Cnih3*$^{+/+}$ *vs. female Cnih3*$^{+/+}$ *p = 0.5516*).

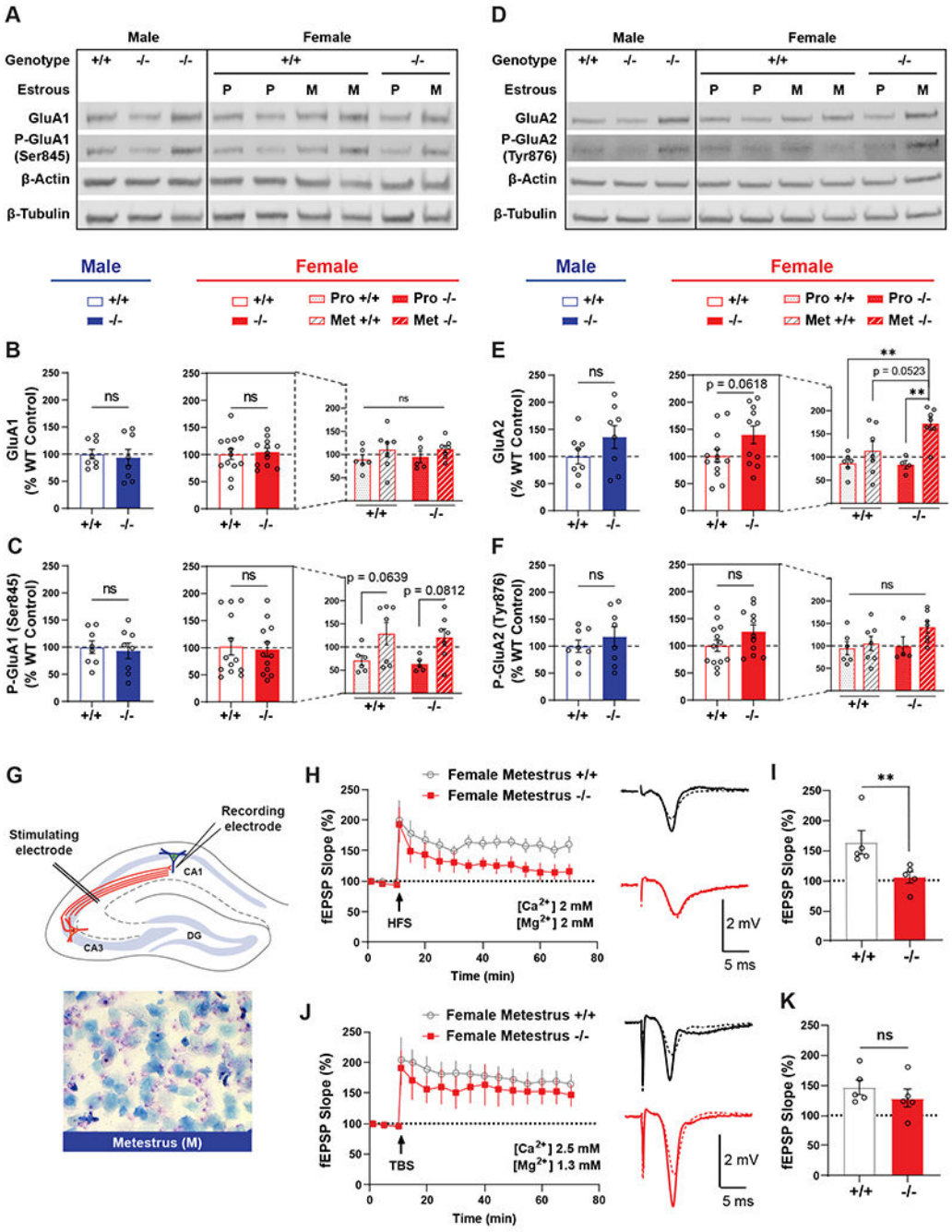

Figure 6: Altered AMPAR subunit composition and attenuated synaptic plasticity were observed in the Schaffer Collateral (SC) pathway of the dHPC in *Cnih3*$^{-/-}$ female mice during metestrus

(A) Example western blot images from male and female *Cnih3*$^{+/+}$ (male: n = 8; female: n = 13) and *Cnih3*$^{-/-}$ (male: n = 8; female: n = 12) animals. Each lane represents dHPC synaptosomal fractions obtained from a single animal. Female samples were collected during proestrus and metestrus stages for both *Cnih3*$^{+/+}$ (proestrus: n = 6; metestrus: n = 7) and *Cnih3*$^{-/-}$ (proestrus: n = 5; metestrus: n = 7) genotypes. In both the female *Cnih3*$^{+/+}$ and *Cnih3*$^{-/-}$ proestrus datasets, one sample was removed from the analysis due to incorrect estrous cycle stage. Blots were probed for GluA1, P-GluA1 (Ser845), and HKPs

β-actin (used for normalization) and β-tubulin. Datasets were normalized to within-sex and within-blot *Cnih3*$^{+/+}$ controls, data is shown as normalized percentages to the baseline average of *Cnih3*$^{+/+}$ controls (set at 100%). (B) Quantification of GluA1 separated by sex (*Two-tailed unpaired t test, Cnih3*$^{+/+}$ *vs. Cnih3*$^{-/-}$*: male: p = 0.7734, female: p = 0.7579; if normalize female Cnih3*$^{+/+}$ *to male Cnih3*$^{+/+}$ *average: male Cnih3*$^{+/+}$ *vs. female Cnih3*$^{+/+}$ *p = 0.8245*) and estrous cycle stage (*Two-way ANOVA,* ***Estrous****: $F_{(1, 21)} = 2.395$, p = 0.1367;* ***Genotype****: $F_{(1, 21)} = 0.07012$, p = 0.7937;* ***Estrous x Genotype****: $F_{(1, 21)} = 0.03265$, p = 0.8583*). (C) P-GluA1 (Ser845) separated by sex (*Two-tailed unpaired t test, male: p = 0.7284, female: Cnih3*$^{+/+}$ *combined female dataset did not pass the Shapiro-Wilk normality test, nonparametric two-tailed Mann-Whitney test, p = 0.9362; if normalize female Cnih3*$^{+/+}$ *to male Cnih3*$^{+/+}$ *average: male Cnih3*$^{+/+}$ *vs. female Cnih3*$^{+/+}$ *p = 0.4558*) and estrous cycle stage (*Two-way ANOVA,* ***Estrous****: $F_{(1, 21)} = 9.935$, p = 0.0048;* ***Genotype****: $F_{(1, 21)} = 0.1828$, p = 0.6734;* ***Estrous x Genotype****: $F_{(1, 21)} = 6.723e^{-6}$, p = 0.9980; Post-hoc Sidak's multiple comparisons test between proestrus and metestrus, Cnih3*$^{+/+}$*: p = 0.0639; Cnih3*$^{-/-}$*: p = 0.0812*). (D) Example western blots from the same samples used in panels A – C, probed for GluA2, P-GluA1 (Tyr876), and HKPs β-actin (used for normalization) and β-tubulin (used for normalization in one blot due to inconsistent actin staining). (E) Quantification of GluA2 separated by sex (see Table S1 for relevant statistical outlier) (*Two-tailed unpaired t test, male: p = 0.1769, female: p = 0.0618)* and estrous cycle stage (*Two-way ANOVA,* ***Estrous****: $F_{(1, 20)} = 13.45$, p = 0.0015;* ***Genotype****: $F_{(1, 20)} = 3.077$, p = 0.0947;* ***Estrous x Genotype****: $F_{(1, 20)} = 3.768$, p = 0.0665; post-hoc Sidak's multiple comparisons test, p = 0.0076 compared to Cnih3*$^{+/+}$ *females in proestrus, p = 0.0035 compared to Cnih3*$^{-/-}$ *females in proestrus, p = 0.0523 compared to Cnih3*$^{+/+}$ *females in metestrus*). (F) P-GluA2 (Tyr876) separated by sex (*Two-tailed unpaired t test, male: p = 0.9800, female: p = 0.1243)* and estrous cycle stage (*Two-way ANOVA,* ***Estrous****: $F_{(1, 20)}$, = 2.698, p = 0.1161;* ***Genotype****: $F_{(1, 20)} = 1.630$, p = 0.2163;* ***Estrous x Genotype****: $F_{(1, 20)} = 0.9555$, p = 0.3400*). (G) Schematic of field potential recording from the SC pathway of the dHPC in slice. Female mice were chosen for LTP experiments during the metestrus phase due to memory deficits and biochemical dysregulation observed during this stage in *Cnih3*$^{-/-}$ female mice. Representative image of a stained vaginal lavage sample from a female animal in metestrus. (H) Time course of LTP under standard conditions (2 mM Ca^{2+}, 2 mM Mg^{2+} in ASCF) for *Cnih3*$^{+/+}$ (n = 5) and *Cnih3*$^{-/-}$ female mice (n = 5) in the metestrus stage of the estrous cycle. Following 10 min of baseline fEPSPs, the SC pathway was subjected to HFS to induce LTP (1 min after HFS stimulation, *Two-tailed unpaired t test, p = 0.8703*). (I) Comparison of half-maximal fEPSP slope (presented as % baseline) 1 hr post-HFS between *Cnih3*$^{+/+}$ and *Cnih3*$^{-/-}$ metestrus females (*two-tailed Mann-Whitney test, p = 0.0079*). (J) Time course of LTP under higher Ca^{2+} and lower Mg^{2+} conditions during TBS (2.5 mM Ca^{2+}, 1.3 mM Mg^{2+} in ASCF) for *Cnih3*$^{+/+}$ (n = 5) and *Cnih3*$^{-/-}$ female mice (n = 5) in the metestrus stage of the estrous cycle. TBS was applied after 10 min of baseline recordings to induce LTP. (K) Comparison of half-maximal fEPSP slope 1 hr post-TBS under high Ca^{2+} conditions between *Cnih3*$^{+/+}$ and *Cnih3*$^{-/-}$ metestrus female mice (*Unpaired two-tailed t test, p = 0.3711*).

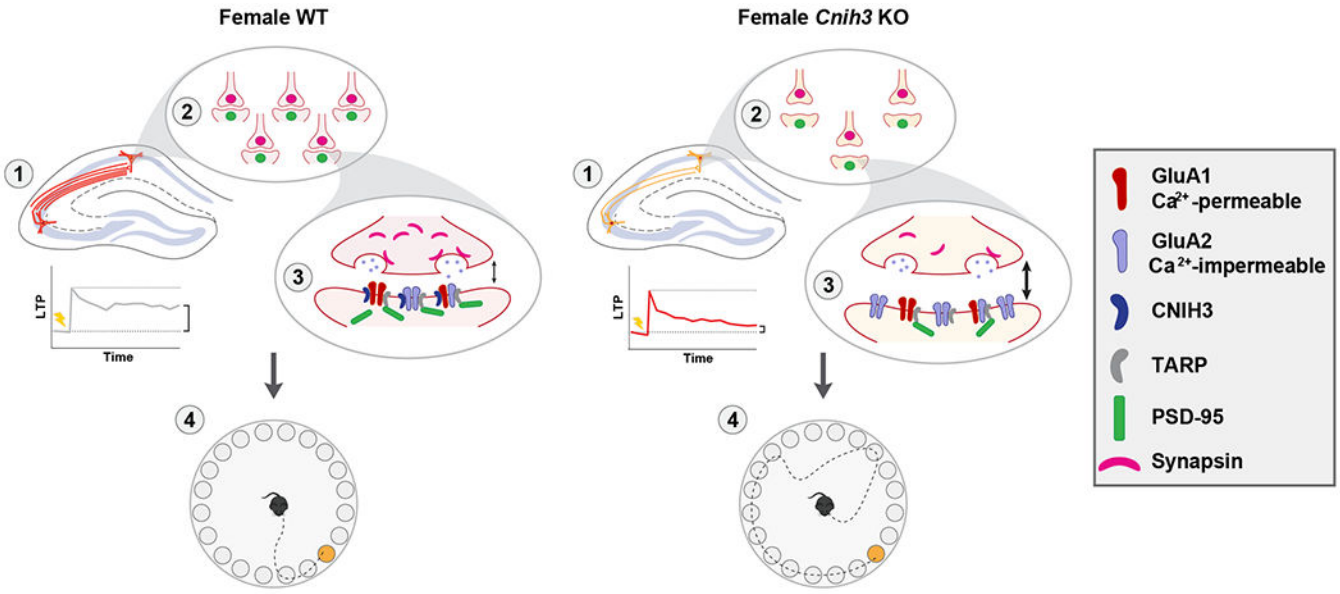

Figure 7: Summary of results

In this study we report altered spatial memory and hippocampal processes between female WT and female *Cnih3* KO mice, with no effect of CNIH3 in male animals. In summary, we observed: (1) attenuated LTP in the SC pathway of the dHPC, (2) a reduction in synaptic markers and overall synaptic density in the dorsal CA1, in addition to increased distance between PSD-95 (green) and Synapsin (magenta) puncta within synaptic loci, and (3) increased GluA2-containing Ca^{2+}-impermeable AMPARs in the dHPC synaptosome in female *Cnih3* KO mice (especially during metestrus). (4) We propose that these changes in the dHPC underlie the short-term spatial memory deficits that we observed in female *Cnih3* KO mice in the Barnes maze.

KEY RESOURCES TABLE

Resource Type	Specific Reagent or Resource	Source or Reference	Identifiers	Additional Information
Add additional rows as needed for each resource type	**Include species and sex when applicable.**	**Include name of manufacturer, company, repository, individual, or research lab. Include PMID or DOI for references; use "this paper" if new.**	**Include catalog numbers, stock numbers, database IDs or accession numbers, and/or RRIDs. RRIDs are highly encouraged; search for RRIDs at https://scicrunch.org/resources.**	**Include any additional information or notes if necessary.**
Antibody	Guinea Pig anti-Synapsin 1/2	Synaptic Systems	#106 004, RRID: AB_1106784	
Antibody	Goat anti-PSD95	Abcam	ab12093, RRID: AB_298846	
Antibody	Rabbit anti-myc-tag	Cell Signaling Technology	#2272, RRID: AB_10692100	
Antibody	Donkey anti-goat 594 Alexa Fluor	Life Technologies	#A-11058, RRID: AB_2534105	
Antibody	Goat anti-guinea pig 488 Alexa Fluor	Life Technologies	#A-11073, RRID: AB_2534117	
Antibody	Goat anti-rabbit 594 Alexa Fluor	Life Technologies	#A-11037, RRID:AB_2534095	
Antibody	Rabbit anti-PSD95	Cell Signaling Technology	#3409, RRID:AB_1264242	
Antibody	Mouse anti-GluA1	Abcam	ab174785	
Antibody	Rabbit anti-phospho-GluA1 (Ser845)	Cell Signaling Technology	#8084, RRID:AB_10860773	
Antibody	Mouse anti-GluA2	Millipore	MABN1189, RRID:AB_2737079	
Antibody	Mouse anti-phospho-GluA2 (Tyr876)	Cell Signaling Technology	#4027, RRID:AB_1147622	
Antibody	Rabbit anti-beta III tubulin	Millipore	AB15708, RRID:AB_838246	
Antibody	Mouse anti-beta actin	Millipore	MAB1501, RRID:AB_2223041	
Antibody	IRDye 680RD Donkey anti-guinea pig IgG	LI-COR Biosciences	926-68077, RRID:AB_10956079	
Antibody	IRDye 680RD Donkey anti-mouse IgG	LI-COR Biosciences	926-68072, RRID:AB_10953628	
Antibody	IRDye 800CW Donkey anti-rabbit IgG	LI-COR Biosciences	925-32213, RRID:AB_2715510	
Bacterial or Viral Strain	AAV5-CAMKII-eYFP	Virus Vector Core, The University of North Carolina at Chapel Hill	N/A	
Bacterial or Viral Strain	AAV5-CAMKII-myc-CNIH3-t2a-GFP virus	This paper, Hope Center Viral Core at Washington University in St. Louis	N/A	
Biological Sample	Mouse brain tissue	This paper	N/A	
Biological Sample	Mouse vaginal smears	This paper	N/A	
Commercial Assay Or Kit	RNeasy Mini Kit	Qiagen	#74004	
Commercial Assay Or Kit	iScript Reverse Transcriptase Supermix	BIO-RAD	#1708840	
Commercial Assay Or Kit	PowerUp SYBR Green Master Mix	Applied Biosystems	#A25742	
Commercial Assay Or Kit	Pierce BCA Protein Assay Kit	ThermoFisher Scientific	#23225	
Commercial Assay Or Kit	Revert 700 Total Protein Stain and Wash Solution Kit	LI-COR Biosciences	#926-11010	

Resource Type	Specific Reagent or Resource	Source or Reference	Identifiers	Additional Information
Add additional rows as needed for each resource type	**Include species and sex when applicable.**	**Include name of manufacturer, company, repository, individual, or research lab. Include PMID or DOI for references; use "this paper" if new.**	**Include catalog numbers, stock numbers, database IDs or accession numbers, and/or RRIDs. RRIDs are highly encouraged; search for RRIDs at https://scicrunch.org/resources.**	**Include any additional information or notes if necessary.**
Organism/Strain	C57BL/6 mice, male and female	Wild-type, local colony bred from breeders obtained from The Jackson Laboratory	RRID:IMSR_JAX:000664	
Organism/Strain	*Cnih3*$^{tm1a(KOMP)Wtsi}$ C57BL/6 mice, male and female	Knockout Mouse Project	RRID:MMRRC_053868-UCD	
Organism/Strain	*Cnih3*$^{-/-}$ C57BL/6 mice, male and female	This paper	N/A	
Sequence-Based Reagent	Primers for RT-qPCR, see Supplemental Methods	This Paper, Integrated DNA Technologies	N/A	
Software; Algorithm	Any-Maze	Stoelting	**RRID:SCR_014289**	
Software; Algorithm	pClamp & Clampfit	Molecular Devices	**RRID:SCR_011323**	
Software; Algorithm	Zen Software	Carl Zeiss Microscopy	**RRID:SCR_018163**	
Software; Algorithm	Applied Biosystems QuantStudio 6 PCR System	Applied Biosystems	**RRID:SCR_020239**	
Software; Algorithm	Leica Application Suite X	Leica Microsystems	**RRID:SCR_013673**	
Software; Algorithm	LI-COR Image Studio Software	LI-COR Biosciences	**RRID:SCR_015795**	
Software; Algorithm	Imaris	Bitplane	**RRID:SCR_007370**	
Software; Algorithm	GraphPad Prism v9	GraphPad Software	**RRID:SCR_002798**	
Software; Algorithm	MATLAB v9.1, Custom Code	Mathworks, Sauerbeck et al., 2020 Neuron, and Reitz et al., 2021 STAR Protoc.	RRID:SCR_001622, https://github.com/KummerLab/SEQUIN	